

# Enhancing Multiuser MIMO Through Opportunistic D2D Cooperation

Can Karakus    Suhas Diggavi

## Abstract

We propose a cellular architecture that combines multiuser MIMO (MU-MIMO) downlink with opportunistic use of unlicensed ISM bands to establish device-to-device (D2D) cooperation. The architecture consists of a physical-layer cooperation scheme based on forming downlink virtual MIMO channels through D2D relaying, and a novel resource allocation strategy for such D2D-enabled networks. We prove the approximate optimality of the physical-layer scheme, and demonstrate that such cooperation boosts the effective SNR of the weakest user in the system, especially in the many-user regime, due to multiuser diversity. To harness this physical-layer scheme, we formulate the cooperative user scheduling and relay selection problem using the network utility maximization framework. For such a cooperative network, we propose a novel utility metric that jointly captures fairness in throughput and the cost of relaying in the system. We propose a joint user scheduling and relay selection algorithm, which we prove to be asymptotically optimal. We study the architecture through system-level simulations over a wide range of scenarios. The highlight of these simulations is an approximately  $6\times$  improvement in data rate for cell-edge (bottom fifth-percentile) users (over the state-of-the-art) while still improving the overall throughput, and taking into account various system constraints.

## I. INTRODUCTION

One of the biggest challenges in wireless networks is to provide uniform connectivity experience throughout the service area. The problem is especially difficult at the cell-edge, where users with unfavorable channel conditions need to receive reliable and high-rate communications. One of the ambitious visions of 5G network design is to achieve  $10\times$  reduction in data rate variability in the cell (over the state-of-the-art), without sacrificing the overall sum throughput in the system. In this paper, we propose and study a solution that, realistic simulations indicate,

The authors are with the Department of Electrical Engineering, University of California, Los Angeles. E-mail: {karakus, suhasdiggavi}@ucla.edu. This work was supported in part by NSF grants #1314937 and #1514531 and a gift from Intel.

can give up to approximately  $6\times$  improvement in data rate for cell-edge (bottom fifth-percentile) users while still improving the overall throughput under various system constraints.

The proposed solution is centered around opportunistically using the unlicensed band through device-to-device (D2D) cooperation to improve the performance of the licensed multiple-antenna downlink transmission. This solution can be enabled without the presence of any WiFi hotspots, or other data offloading mechanisms. The main idea is an architecture where a multiple-antenna downlink channel is enhanced through out-of-band D2D cooperation, which is opportunistically harnessed through scheduling algorithms designed for this architecture.

At the physical layer, the proposed architecture uses D2D relaying to provide the user with multiple versions of the downlink channel outputs, forming virtual MIMO links. In doing so, we exploit the orthogonality of the D2D links to simplify coding. We then use the utility maximization framework to develop a resource allocation algorithm specifically tailored to downlink with D2D cooperation, which opportunistically schedules the use of such D2D links in a centralized manner to maximize the gains, while accounting for fairness between users, the cost of cooperation, and potential conflicts between multiple D2D transmissions. Extensive simulations based on 3GPP channel models demonstrate that the proposed architecture can yield up to approximately  $6\times$  throughput gain for the bottom fifth-percentile of users in the network and up to approximately  $4\times$  gain for median users over the state-of-the-art single-user MIMO (SU-MIMO), without degrading the throughput of the high-end users.

The architecture is predicated on two opposing developments. The first is that infrastructure is becoming more powerful, with the use of a growing number of multiple antennas through massive MIMO. The other development is on the user equipment (UE) side, with mobile devices becoming more powerful, both in terms of spectrum access and computational power. Most of the mobile devices currently in widespread use can access multiple bands over the ISM spectrum, including the 2.4GHz and 5GHz bands. Technologies such as WiFi Direct and Bluetooth readily implement D2D communication over these unlicensed bands. Furthermore, dense clusters of users constitute a challenging scenario for increasing capacity through massive MIMO, which is precisely the scenario where D2D cooperation is the most useful, since the D2D links are much stronger. Our proposed architecture leverages these developments and the geographical clustering of users to combine MU-MIMO with opportunistically enabled D2D cooperation to achieve significant cell-edge gains.

Since the architecture relies on opportunistically using the unlicensed ISM bands, an important question is how the D2D transmissions would affect other wireless technologies using the

unlicensed bands, mainly WiFi and LTE-Unlicensed (LTE-U). As a co-existence mechanism with existing WiFi and LTE-U networks, we propose a simple back-off strategy, where users that are within the range of ongoing WiFi access point or LTE-U small cell transmissions are unavailable for D2D cooperation. In practice, this can be implemented through a strategy similar to LTE-U [20]: a user can search for an available (unused) channel within the unlicensed band to use for D2D cooperation. If none exists, the user can simply declare itself unavailable for D2D cooperation, or transmit only for a short duty cycle. This is in line with the main philosophy of using D2D cooperation, which is helpful especially for users with poor reception, at the cell edge or who do not have access to a mechanism to boost the capacity (*e.g.*, small cell, WiFi access point etc.). Any interference between D2D and other networks despite this back-off mechanism is still taken into account in our analysis and simulations through *intermittent availability* of resources. Our results show that despite the interference, the throughput loss in WiFi users is small compared to the gains in the cell-edge users, since the fraction of time D2D transmission is required from a given user is small. We find that the performance of the system where WiFi and D2D are simultaneously enabled strictly dominates the case where each of them is individually enabled, across all percentiles, which supports the case that D2D cooperation can be thought of as a complementary technology to WiFi and LTE-U.

The main technical contributions of the work can be summarized as follows.

- We propose a physical-layer scheme based on D2D relaying and MIMO Tx/Rx processing that approximately achieves (within 2 bits/s/Hz) the capacity of two-user downlink channel with D2D side-channel cooperation (Section III-B) and extend the proposed scheme to MU-MIMO with D2D cooperation (Section III-C). We characterize the gains in terms of cell-edge SNR-scaling due to D2D cooperation for a specific model of clustered networks (Section III-D).
- We formulate the problem of allocating such D2D links for cooperation within the utility maximization framework (Section IV-A). Since the existing cross-layer design tools are not directly applicable in our scenario when D2D transmission conflicts are taken into account, we propose a novel scheduling policy for such D2D-enabled networks (Section IV-B), that takes into account such conflicts. The policy consists of an extension of the single-user scheduling algorithm of [1] to the cooperative MU-MIMO scenario with incomplete network state knowledge, and a novel flow control component based on an explicit characterization of an inner bound on the stability region of the system. The proposed algorithm is shown to be optimal with respect to this inner bound on the stability region (Section IV-D). Our proof

of optimality extends and generalizes the stochastic approximation techniques from [1], [2]. We introduce a novel class of utility functions that incorporate the cost of cooperation and leads to desirable fairness properties, and as such generalizes the conventional utility metrics that are used, such as proportional fairness, to the cooperative scenario (Section IV-C). We also present a low-complexity greedy algorithm for scheduling similar to the one in [3], which takes insights from the developed utility maximization framework (Section IV-E).

- We present an extensive simulation study using 3GPP specifications to study the performance of the proposed architecture (Section V). The main results include (i) a throughput gain ranging from  $4.3\times$  up to  $5.7\times$  (depending on system constraints, channel estimation accuracy etc.) for the users in bottom fifth-percentile for MU-MIMO with D2D cooperation versus the state-of-the-art SU-MIMO <sup>1</sup>, (ii) a throughput gain ranging from  $3.7\times$  up to  $4.9\times$  for the bottom fifth-percentile users versus non-cooperative MU-MIMO, (iii) A throughput gain ranging between  $2.4\times$  up to  $4.5\times$  for the median user versus non-cooperative SU-MIMO, and between  $1.5\times$  and  $2.3\times$  with respect to non-cooperative MU-MIMO, (iv) A reduction of more than 50% in the amount of relaying in the network through the use of novel utility functions, while minimally degrading the proportional-fair scheduling performance, (v) A basic study of an architecture wherein D2D cooperation coexists (and interferes) with WiFi in the network, where it is shown that despite the presence of off-loading opportunities over the same band, the overall throughput performance of the system is better than when either of WiFi and D2D is individually enabled, across all throughput percentiles.

**Related work:** There is a vast literature on D2D communication in cellular networks (see [4] for a comprehensive survey). A significant part of these works focus on in-band D2D, where the D2D links share the same spectrum with the cellular links. In this architecture, the main challenge is to manage interference and perform optimal resource allocation across cellular and D2D flows. Again, from an architectural viewpoint, a significant part of the works in the D2D literature focus on direct proximal communication between devices, which allows the traffic to skip the infrastructure nodes, potentially reducing delay and the load on the infrastructure. There are two main differences between these works and ours. The first is that we study the use of *out-of-band* D2D, where there is no interference between cellular and D2D transmissions. Moreover, the D2D resources are not dedicated, *i.e.*, other transmissions, such as WiFi, may take

<sup>1</sup>The gain can reach up to  $6.3\times$  when different D2D transmissions are over orthogonal bands and do not interfere with each other.

place over the same band. Second, we focus on *D2D cooperation* as opposed to *communication*. In other words, the devices themselves do not have messages for each other; they simply use their D2D capability to assist downlink message flows intended for other devices.

Conceptually, the most relevant work in the literature to our problem is the one in [5], where the authors propose an architecture where users form clusters through the use of unlicensed bands, designate the user with the best channel as the cluster head, and all communication with the base station is performed through the cluster head. The authors propose a cluster scheduling algorithm, where the base station treats each cluster as a single user. In contrast to these works, our physical-layer scheme is not based on routing; it explicitly uses the direct link from the base station to the destination user in addition to the relay links. We also consider a much more general scheduling algorithm based on utility optimization, accounting for fairness and cooperation cost. Further, we do not assume *a priori* designated clusters, and relays are assigned dynamically to users at each time slot, based on current channel conditions,.

User scheduling for downlink MU-MIMO has been studied extensively [6], [7], [3], [8]. The works in [6], [7] focus on overall throughput maximization, and study the asymptotic regime as the number of users tend to infinity. Low-complexity greedy approximations to such algorithms was considered in [3]. The work in [8] study the MU-MIMO scheduling problem within the utility maximization framework, under imperfect network state information. This work uses the cross-layer control framework presented in [9], based on virtual queues. As will be explained in Section IV, this framework does not immediately extend to our setup; instead, we generalize the single-user scheduling scheme in [1] to our cooperative MU-MIMO setup.

**Paper outline:** In Section II, we present our model and high-level description of the proposed architecture, and explain some of the notation that is used throughout the paper. In Section III, we present the physical-layer cooperation scheme, prove its approximate optimality, describe its extension to MU-MIMO, and study the scaling behavior of the minimum effective SNR in the network as a function of number of users. In Section IV, we formulate the downlink cooperative scheduling problem within the utility optimization framework, present an optimal algorithm and its greedy approximation for reduced computational complexity. In Section V, we present our simulation results, and in Section VI, we state the concluding remarks.

## II. MODEL AND DEFINITIONS

We consider the downlink of a cellular communication system consisting of a single cell (we will consider multi-cell systems in the simulations in Section V), with a base station equipped

TABLE I: Notation for variables corresponding to the D2D link  $(i, j)$ 

Notation	Explanation	Notation	Explanation
$g_{ij}$	D2D channel gain	$Q_{ij}$	State of the queue at relay $j$ for destination $i$
$\phi_{ij}$	Path-loss factor	$\mu_{ij}$	Binary service process (transmission permission indicator) for the queue $Q_{ij}$
$\nu_{ij}$	Fading parameter	$A_{ij}$	Binary arrival process (D2D link scheduling indicator) for the queue $Q_{ij}$
$B_{ij}$	D2D link availability indicator	$J_{ij}$	D2D interference indicator
$C_{ij}$	The capacity of the D2D link	$\beta_{ij}$	Arrival rate to the queue $Q_{ij}$

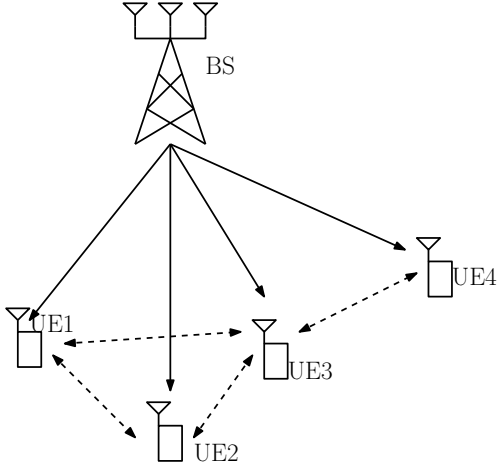


Fig. 1: The downlink network with side-channels

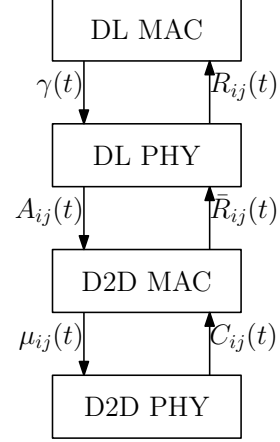


Fig. 2: The layers operating at each node, and the interactions between them

with  $M$  antennas, and a set  $\mathcal{N}$  of single-antenna users, where  $|\mathcal{N}| = n$  (see Fig. 1). The network architecture consists of the layers shown in Figure 2. We assume slotted time, with  $m$  representing the downlink physical-layer time index, and  $t$  representing the downlink MAC-layer time index, where a MAC-layer time slot consists of  $T$  physical-layer slots<sup>2</sup>. We will use the notation  $m \sqsubset t$  to mean that the physical-layer slot  $m$  lies within the MAC-layer slot  $t$ , *i.e.*,  $(t-1)T < m \leq tT$ .

We will next describe the models corresponding to each layer.

#### A. D2D Physical Layer

For any pair  $(i, j) \in \mathcal{N}^2, i \neq j$ , we assume a link with time-variant channel gain  $g_{ij}(t) = \sqrt{\phi_{ij}}\nu_{ij}(t)$ , where  $\phi_{ij} \in \mathbb{R}$  is the path loss component, and  $\nu_{ij}(t) \sim \mathcal{CN}(0, 1)$  is the fading component for the pair  $(i, j)$ , i.i.d. across MAC layer slots. We assume reciprocal side-channels, *i.e.*,  $g_{ij}(t) = g_{ji}(t)$ , and define  $N(t) := \{\nu_{ij}(t)\}_{i,j}$  and  $\Phi := \{\phi_{ij}\}_{i,j}$ .

<sup>2</sup>We will use square brackets to denote physical-layer time indices, and round brackets for MAC layer time indices.

The connectivity graph for the set of nodes  $\mathcal{N}$  is a graph  $\mathcal{G} = (\mathcal{V}, \mathcal{E})$  such that  $\mathcal{V} = \mathcal{N}$ , and  $\mathcal{E}$  is such that  $(i, j) \in \mathcal{E}$  if  $i = j$  or  $\phi_{ij} > \theta$  for some threshold  $\theta > 0$  (e.g., noise level).

We further define the conflict graph  $\mathcal{G}_c = (\mathcal{V}_c, \mathcal{E}_c)$  such that

$$\begin{aligned} \mathcal{V}_c &:= \{(i, j) \in [n]^2 : i \neq j\} \\ \mathcal{E}_c &:= \{((i, j), (k, \ell)) : (i, j) \neq (k, \ell) \text{ and } ((i, \ell) \in \mathcal{E} \text{ or } (j, k) \in \mathcal{E})\}. \end{aligned} \quad (1)$$

The conflict graph represents the pairs of message flows  $(i, j), (k, \ell)$  that are not allowed to simultaneously transmit due to interference. In particular, the interference model that induces the conflict graph  $\mathcal{G}_c$  as defined in (1) is similar to the two-hop interference model of [10], [11], but also takes into account the directionality of the transmission. Note that under this model, if the interference link strength is below the threshold  $\theta$ , then it is ignored.

We note that the path-loss parameters between user pairs are sufficient to generate the connectivity graph and the conflict graph using their definitions, and thus the base station has access to the full structure of these graphs.

The channel from user  $j \in \mathcal{N}$  to user  $i \in \mathcal{N} - \{j\}$  is then modeled by

$$\bar{y}_i[m] = B_{ij}(t)J_{ij}(t) (g_{ij}(t)x_j[m] + \bar{z}_i[m])$$

for  $m \sqsubset t$ , where

$$J_{ij}(t) = \begin{cases} 0, & \text{if } \exists(k, \ell) \text{ s.t. } ((i, j), (k, \ell)) \in \mathcal{E}_c \text{ and } \|x_\ell[\tilde{m}]\|^2 > 0 \text{ for some } \tilde{m} \sqsubset t \\ 1, & \text{otherwise} \end{cases},$$

$\bar{y}_i[m]$  is the output of the side-channel at user  $i$ ,  $x_j[m] \in \mathbb{C}$  is the input from user  $j$  at time  $m$ ,  $\bar{z}_i[m] \sim \mathcal{CN}(0, 1)$  is the circularly symmetric complex white Gaussian noise process, and  $B_{ij}(t)$ , for each  $t$ , is a *Bernoulli*( $p_{ij}$ ) random variable, representing the availability of the link  $(i, j)$ <sup>3</sup>. We define  $B(t) := \{B_{ij}(t)\}_{i \neq j}$ . We assume an average power constraint  $\frac{1}{T} \sum_{m=1}^T \|x_j[m]\|^2 \leq 1$ , absorbing the input power into the channel gain. The capacity of the D2D link  $(i, j)$  corresponding to the channel realization at time  $t$  is given by  $C_{ij}(t) := \log(1 + \|g_{ij}(t)\|^2)$ .

We assume the base station has knowledge of the average SNR, *i.e.*, the path-loss component  $\phi_{ij}$  for each  $(i, j)$  pair, but has no knowledge of the fading realization  $\nu_{ij}(t)$ , or the link availability  $B_{ij}(t)$ . The assumption that the average D2D SNR is known at the base station is reasonable since D2D links are SISO, and since the phase of the D2D channel is not required,

<sup>3</sup>Since the side-channels are over unlicensed bands, there could potentially be other transmissions (e.g., WiFi access points etc.) in the same band in the vicinity of a user, thus making the link *unavailable* intermittently. Note that this is in addition to the unavailability modeled by  $J_{ij}(t)$ , which corresponds to interfering links *in the network*  $\mathcal{N}$ .

the base station only needs to know a single, long-term averaged SNR parameter for each pair of users, which is low overhead. Further, since SNR varies significantly slower than the phase of the channel, the devices do not need to report this value to the base station very often. Moreover, since there is typically a small number of users in the range of a given user, in practice each user only needs to report D2D SNR for a small number of D2D links (that can be predefined in the protocol), as opposed to every possible pair of users.

This is because these parameters might change relatively fast compared to the time scale of a cellular subframe, leaving little time to report them to the base station. Note that the knowledge of  $\Phi$  is sufficient to infer the full structure of the graphs  $\mathcal{G}$  and  $\mathcal{G}_c$ .

### B. D2D MAC Layer

We assume that each node  $j \in \mathcal{N}$  maintains  $(n - 1)$  queues, whose states are given by  $Q_{ij}(t)$ ,  $i \in \mathcal{N} - \{j\}$ , each representing the number of slots of transmission<sup>4</sup> to be delivered to node  $i$ . We assume the queue states evolve according to

$$Q_{ij}(t + 1) = (Q_{ij}(t) - B_{ij}(t)J_{ij}(t)\mu_{ij}(t))^+ + A_{ij}(t), \quad (2)$$

where  $\mu_{ij}(t)$  is the service process that takes values in the set  $\{0, 1\}$ , and is induced by the multiple-access protocol  $\mathcal{I}$  used by the nodes, indicating whether or not the flow  $(i, j)$  is granted permission for transmission at time  $t$ .  $A_{ij}(t)$  is the arrival process for queue  $(i, j)$ , representing whether new data has been scheduled for transmission from user  $j$  to user  $i$ . We define the average arrival rates as  $\beta_{ij}(t) := \frac{1}{t} \sum_{\tau=1}^t A_{ij}(\tau)$ , and  $\beta_{ij} := \limsup_{t \rightarrow \infty} \beta_{ij}(t)$ . For a given vector of arrival rates  $\beta := \{\beta_{i,j}\}_{i \neq j}$ , the system is said to be *stable* if the average queue sizes are bounded, *i.e.*, for all  $(i, j)$ ,  $\limsup_{t \rightarrow \infty} \mathbb{E}[Q_{ij}(t)] < \infty$ . The set of arrival-rate vectors  $\beta$  for which there exists service processes  $\{\mu_{ij}(t)\}_{i \neq j}$  such that the system is stable is called the *stability region* of the queueing system, and will be denoted by  $\Lambda$ .

In this paper, we do not deal with the lower-level details of the multiple-access protocol  $\mathcal{I}$ , but we assume the following:

- 1)  $J_{ij}(t)\mu_{ij}(t) = \mu_{ij}(t)$ , *i.e.*, transmission is not attempted if the channel is not available due to an interference constraint.
- 2) Protocol  $\mathcal{I}$  achieves the stability region  $\Lambda$  of the system.

<sup>4</sup>Note that  $Q_{ij}(t)$  does not represent the number of *bits* to be transmitted, but the number of *slots of transmission*. This is because the reception of relay does not directly translate into information bits, but is rather a *refinement* of the reception of the destination node.



Note that in a completely distributed system, the first condition may not be satisfied due to the hidden terminal problem. However, since the nodes are already in communication with the base station, and the base station has complete knowledge of the conflict graph  $\mathcal{G}_c$ , this problem can be circumvented with appropriate control signaling with the base station. Under the first assumption, one can design stability-region-achieving protocols  $\mathcal{I}$  that are centralized such as backpressure scheduling [12]; distributed, such as CSMA-type algorithms [13], [10], [14]; or semi-centralized, by coordinating with the base station in varying degrees.

### C. Downlink Physical Layer

The downlink channel output of user  $i \in \mathcal{N}$  at time  $m \in \mathbb{N}$ ,  $y_i[m]$ , is given by

$$y_i[m] = \mathbf{h}_i^*(t)\mathbf{x}[m] + z[m] \quad (3)$$

for  $m \sqsubset t$ , where  $\mathbf{h}_i(t) \in \mathbb{C}^M$  is the time-variant complex channel vector of user  $j$  at time  $t$ ,  $\mathbf{x}[m]$  is the input vector to the channel at time  $m$ , and  $z[m] \sim \mathcal{CN}(0, 1)$  is the circularly symmetric complex white Gaussian noise process. We assume a long-term average power constraint  $\frac{1}{T} \sum_{m=1}^T \text{tr}(\mathbf{x}[m]\mathbf{x}^*[m]) \leq 1$ , and define  $H(t) := \{\mathbf{h}_i(t)\}_i$ .

We assume that there is an underlying incremental redundancy scheme such as hybrid ARQ employed in the system. For simplicity, we assume the idealized scenario where even though the resource allocation and transmission decisions of the base station cannot depend on the unknown components of the network state, *i.e.*,  $(N(t), B(t))$ , once these decisions are fixed and the transmission is performed, the capacity corresponding to these decisions and the actual realization of the network state at time  $t$  is achievable. This is similar to the optimistic rate assumption<sup>5</sup> in [8].

We assume the vector of arrival rates  $\beta$  to the D2D MAC-layer queues lies within the stability region  $\Lambda$  of these queues. Then, in order to abstract the D2D links in the downlink physical layer, for each  $(i, j)$ , we can assume that a noiseless link with capacity  $\bar{R}_{ij}(t)$  is available at time  $t$ , where  $\bar{R}_{ij}(t) = C_{ij}(\tau)$  for some finite  $\tau \geq t$ . Note that at time  $t$ , the base station has no knowledge of  $C_{ij}(\tau)$ , but can still compute the average capacity  $\mathbb{E}_{N(\tau)}[C_{ij}(\tau) | \phi_{ij}]$  for a given link  $(i, j)$ , for a transmission decision. We define  $\bar{N}(t) = N(\tau)$ .

We denote the instantaneous information-theoretic capacity region of the channel (3) combined with the set of links  $(i, j)$  with capacities  $\bar{R}_{ij}(t)$  at time  $t$ , conditioned on a particular realization

<sup>5</sup>As discussed in [8], this can also be implemented through a rate adaptation scheme, *e.g.*, as in [15].

$\{\bar{N}(t) = m\}$  as  $\mathcal{C}_m(t)$ . A physical-layer strategy  $\gamma$  is a map

$$(H(t), \Phi, \bar{N}(t)) \mapsto \{R_{ij}(t)\}_{i,j}$$

such that

- 1)  $R_{ij}(t) > 0$  only if  $A_{ij}(t) = 1$  (see Table I).
- 2) For all  $m$ , the induced map  $\gamma_m : (H(t), \Phi, m) \mapsto \{R_{ij}^m(t)\}_{i,j}$  is such that  $\{R_i^m(t)\}_i \in \mathcal{C}_m(t)$ , where  $R_i^m(t) := \sum_j R_{ij}^m(t)$ , and  $R_{ij}^m(t)$  is the rate at which data for user  $i$  is transmitted with the help of user  $j$ , given that  $\bar{N}(t) = m$ .

Note that in general, the individual capacity regions in the set  $\{\mathcal{C}_m\}$  may not be simultaneously achievable with a given fixed strategy  $\gamma$ , since the transmission of the base station only depends on  $(H(t), \Phi)$ . Therefore, a transmission scheme that fits this definition is not necessarily feasible, though the converse holds true.

#### D. Downlink MAC Layer

We are now ready to set up the scheduling problem for the downlink. The long-term average rate of user  $i$  up to time  $t$  is defined as  $r_i(t) = \frac{1}{t} \sum_{\tau=1}^t \sum_{j \in \mathcal{N}} R_{ij}(\tau)$ , and the long-term throughput of user  $i$  is  $r_i = \liminf_{t \rightarrow \infty} r_i(t)$ . Define  $\mathbf{r}(t) = \{r_i(t)\}_i$ .

We assume an infinite backlog of data to be transmitted to each user  $i \in \mathcal{N}$ . Given the D2D MAC protocol  $\mathcal{I}$  and a set of physical-layer strategies  $\Gamma$ , at every time slot  $t$ , the base station chooses a strategy  $\gamma \in \Gamma$ . A scheduling policy  $\pi$  is a collection of mappings

$$(\mathbf{r}(t-1), \beta(t-1), H(t), \Phi) \mapsto \gamma(t),$$

indexed by  $t$ . If  $\beta^\pi$  represents the vector of arrival rates to the queues under policy  $\pi$ , then the policy  $\pi$  is called *stable* if  $\beta^\pi \in \Lambda$ .

### III. DOWNLINK PHYSICAL LAYER: ACHIEVABLE RATES

In this section, we describe a class of physical layer cooperation strategies that will be used as a building block for our proposed architecture, and derive its achievable rates. We will first focus on the two-user case, where we show the approximate information-theoretic optimality of the scheme. We consider the extension to MU-MIMO in Section III-C.

The main idea behind the cooperation strategy is that the D2D side-channel can be used by the destination node to access a quantized version of the channel output of the relay node, which combined with its own channel output, effectively forms a MIMO system. The base station can

perform signaling based on singular value decomposition over this effective MIMO channel, to form two parallel AWGN channels accessible by the destination node. Next, we describe the strategy in detail, and derive the rate it achieves.

### A. Cooperation Strategy

We isolate a particular user pair  $(i, j)$ , and without loss of generality assume  $(i, j) = (1, 2)$ . The effective network model is given by

$$y_i = \mathbf{h}_i^* \mathbf{x} + z_i, \quad i = 1, 2, \quad \hat{y}_2^N = g_2(y_2^N), \quad (4)$$

where we assume user 1 has access to  $\hat{y}_2$ ,  $g$  is a relaying function subject to the entropy constraint  $H(\hat{y}_2^N) \leq N\bar{R}_{12}$  for a block length  $N$ , and the channel parameters  $(\mathbf{h}_1, \mathbf{h}_2, \bar{R}_{12})$  are fixed<sup>6</sup>.

We will make use of the following theorem in what follows.

**Theorem 1** (Wyner-Ziv [16]). *Let  $(y_1, y_2) \sim p(y_1, y_2)$  be an i.i.d. sequence of pairs of random variables over the set  $\mathcal{Y}_1 \times \mathcal{Y}_2$ . Then the rate-distortion function of  $y_2$ , with  $y_1$  available at the decoder is given by*

$$R(D) = \min_{p(w|y_2)} I(y_2; w|y_1)$$

over all conditional distributions  $p(w|y_2)$  with  $w$  taking values over the set  $\mathcal{W}$  such that  $|\mathcal{W}| \leq |\mathcal{Y}_2| + 1$ , and all mappings  $\hat{y}_2(w, y_1)$  such that  $\mathbb{E}[d(\hat{y}_2, y_2)] \leq D$ .

Wyner-Ziv Theorem implies that for a given joint distribution of channel outputs  $p(y_1, y_2)$ , if  $R(D) \leq \bar{R}_{12}$ , then given a block of outputs  $y_2^N$ , user 1 can recover a quantized version  $\hat{y}_2^N$  of outputs such that  $\mathbb{E}[d(\hat{y}_2, y_2)] \leq D$ . This is achieved by performing appropriate quantization and binning of the channel outputs at user 2 (see [16] for details).

Choosing  $\mathbf{x} \sim \mathcal{CN}(\mathbf{0}, \mathbf{Q})$ , i.i.d. over time, we get  $(y_1, y_2) \sim \mathcal{CN}(\mathbf{0}, \Sigma)$  i.i.d. over time, for some covariance matrix  $\Sigma = \mathbf{H}\mathbf{Q}\mathbf{H}^*$  induced by the channel. We further choose  $w = y_2 + q_{12}$ , where  $q_{12} \sim \mathcal{CN}(0, D)$  is independent of all other variables, and we set the mapping  $\hat{y}_2(w, y_1) = w$ . With this set of choices, it can be shown that

$$R(D) = \log \left( 1 + \frac{\sigma_{2|1}^2}{D} \right),$$

<sup>6</sup>We focus on a particular time slot  $t$  to characterize the instantaneous rate achievable.

where  $\sigma_{2|1}^2 = \Sigma_{22} - \Sigma_{21}\Sigma_{11}^{-1}\Sigma_{12}$  is the conditional variance of  $y_2$  given  $y_1$ . Choosing  $D = \frac{\sigma_{2|1}^2}{2^{R_{12}} - 1}$ , it follows that user 1 can access  $\hat{y}_2 = y_2 + q_2$ , where  $q_2 \sim \mathcal{CN}(0, D)$ .

Once user 1 recovers  $\hat{y}_2$ , it can construct the effective MIMO channel

$$\mathbf{y} = \begin{bmatrix} y_1 \\ \hat{y}_2 \end{bmatrix} = \mathbf{H}\mathbf{x} + \begin{bmatrix} z_1 \\ z_2 + q_2 \end{bmatrix}. \quad (5)$$

It follows that all rates  $R < R_{\text{MIMO}}$  are achievable over the effective MIMO channel (5), where

$$R_{\text{MIMO}} = \max_{\text{tr}(\mathbf{Q}) \leq 1} \log |\mathbf{I}_2 + \mathbf{K}^{-1}\mathbf{H}\mathbf{Q}\mathbf{H}^*|,$$

with  $\mathbf{K} = \text{diag}\left(1, 1 + \frac{\sigma_{2|1}^2}{2^{R_{12}} - 1}\right)$ . Note that due to orthogonality of the links incoming to the destination, the encoding and decoding is significantly simplified compared to traditional Gaussian relay channel with superposition, since there is no need for complex schemes such as block Markov encoding and joint decoding, and point-to-point MIMO codes are sufficient from the point of view of the source.

Note that the MIMO channel (5) can be equivalently viewed as  $\min\{M, 2\}$  parallel AWGN channels, using the singular value decomposition (SVD). It will also be useful to lower bound the rates individually achievable over these two parallel streams. Assuming  $\mathbf{H} = \mathbf{U}\mathbf{S}\mathbf{V}^*$  is an SVD, it can be shown that the rates

$$R_{\text{MIMO},k} = \log \left( 1 + \frac{s_k^2 P_k}{1 + |u_{2k}|^2 \frac{\sigma_{2|1}^2}{2^{R_{12}} - 1}} \right), \quad k = 1, 2 \quad (6)$$

are achievable respectively<sup>7</sup>, over the two streams, by transmit beamforming using the matrix  $\mathbf{V}$  and receive beamforming using  $\mathbf{U}^*$ , where  $s_k$  is the  $k$ th singular value,  $u_{2,k}$  is the  $(2, k)$ th element of  $\mathbf{U}$ , and the power allocation parameters satisfy  $P_1 + P_2 \leq 1$ .

*Remark III.1.* The relay channel with orthogonal links from relay to destination and from source to destination was studied by [17] and [18]. In the former, the authors consider a relaying strategy based on decode-and-forward relaying, and focus on performance optimization problems such as optimal bandwidth allocation. The latter work focuses on linear relaying functions for such channels, and characterizes the achievable rates for scalar AWGN case. Here, we propose a relaying scheme based on compress-and-forward [19] that achieves a rate that is within 2 bits/s/Hz of the information-theoretic capacity (as will be shown next) for the MIMO case. Note

<sup>7</sup>We perform the SVD on  $\mathbf{H}$  directly, instead of performing on  $\mathbf{K}^{-1/2}\mathbf{H}$ , in order to obtain closed-form expressions for the subsequent analysis.

that this can also be implemented through quantize-map-forward relaying [21], whose practical implementation is demonstrated in [22].

### B. Gap to Optimality

We next show that the gap between the rate achievable with the cooperation scheme described in the previous subsection and the information-theoretic cut-set upper bound is universally bounded. We first state the cut-set bound, specialized to our channel.

**Theorem 2.** [19] *Any achievable rate  $R$  over the channel described by (4) must satisfy*

$$R < \tilde{C} = \min \left\{ \max_{\text{tr}(\mathbf{Q}) \leq 1} \log |\mathbf{I}_2 + \mathbf{H}\mathbf{Q}\mathbf{H}^*|, \log(1 + \|\mathbf{h}_1\|^2) + \bar{R}_{12} \right\}.$$

Note that the first term in the cut-set bound is simply the capacity of the MIMO channel formed by taking  $\bar{R}_{12} \rightarrow \infty$ , and the second term is the sum of the individual capacities of the D2D side-channel link and the link from base station to user 1.

The following theorem shows that our cooperation strategy achieves a rate within 2 bits/s/Hz of the cut-set bound, for any set of channel parameters and number of antennas.

**Theorem 3.** *For any set of parameters  $(\mathbf{H}, \bar{R}_{12}, M)$ ,  $\tilde{C} \geq R_{MIMO} \geq \tilde{C} - 2$ .*

The proof is provided in the Appendix C.

### C. Cooperation with MU-MIMO

Having analyzed the case with only two users, next we consider the scenario where multiple cooperative pairs are scheduled. In this case, we consider a downlink spatial multiplexing strategy based on MU-MIMO. We will use the strategy described for two users as a building block, and describe a simple extension that easily accommodates any linear beamforming technique.

To this end, we first index all possible downlink streams that can be generated in this way by  $(i, j, k) \in \mathcal{N}^2 \times \{1, 2\}$ , where  $(i, j)$  represents the cooperative pair, and  $k$  represents the stream index corresponding to this pair. We assume  $k \neq 2$  if  $i = j$ , representing the case where user  $i$  is scheduled without a relay.

We assume that an active set  $\mathcal{S} \subseteq \mathcal{N}^2 \times \{1, 2\}$  is scheduled, consisting of such triples  $(i, j, k)$ . Given the set  $\mathcal{S}$ , we create the “virtual users”  $(i, j, k) \in \mathcal{S}$  with the channels

$$\tilde{\mathbf{y}}_{ijk} := \mathbf{u}_{ijk}^* \begin{bmatrix} y_i \\ \hat{y}_j \end{bmatrix} = \mathbf{u}_{ijk}^* \mathbf{H}_{ij} \mathbf{x} + \mathbf{u}_{ijk}^* \begin{bmatrix} z_i \\ z_j + q_{ij} \end{bmatrix} := \tilde{h}_{ijk}^* \mathbf{x} + \tilde{z}_{ijk},$$

where  $\mathbf{H}_{ij} = [\mathbf{h}_i \ \mathbf{h}_j]^*$ , and assuming  $\mathbf{H}_{ij} = \mathbf{U}_{ij} \mathbf{S}_{ij} \mathbf{V}_{ij}^*$  is an SVD of  $\mathbf{H}_{ij}$ ,  $\mathbf{u}_{ijk}$  is the  $k$ th column of  $\mathbf{U}_{ij}$ . By convention, we assume that  $\mathbf{U}_{ii} = \begin{bmatrix} 1 & 0 \end{bmatrix}^*$ . The variance of  $\tilde{z}_{ijk}$  is given by  $1 + |u_{ijk}(2)|^2 D_{ij}$ , where  $u_{ijk}(2)$  is the second element of  $\mathbf{u}_{ijk}$ , and  $D_{ij} = \frac{\sigma_{j|i}^2}{2^{\bar{R}_{ij}-1}}$  is the distortion introduced by quantization at node  $j$ . Note that, when  $i = j$ , we have  $\tilde{\mathbf{h}}_{ijk} = \mathbf{h}_i$ , and we set  $\bar{R}_{ii} = \infty$  so that  $D_{ii} = 0$ .

Note that through the use of SVD over the virtual MIMO channel (5), we have reduced the system into a set of  $|\mathcal{S}|$  single-antenna virtual users with channel vectors  $\frac{1}{1+|u_{ijk}(2)|^2 D_{ij}} \tilde{\mathbf{h}}_{ijk}$ . Given such a set of channel vectors, one can implement any MU-MIMO beamforming strategy (*e.g.*, zero-forcing, conjugate beamforming, SLR maximization etc.), by precoding the transmission with the corresponding beamforming matrix.

#### D. Scaling of SNR Gain in Clustered Networks

In this subsection, we consider a specific clustered network model as an example, and characterize the achievable demodulation SNR gain due to D2D cooperation for the weakest user in the network, under this model. In this analysis, we use several simplifying assumptions on the channel and network model for analytical tractability, in order to get a feel for the scale of the possible gains that can be attained through cooperation. More realistic modeling of the network will be made in the simulations in Section V.

We consider a network where users are clustered in a circular area of radius  $r$ , whose center is a distance  $d$  away from the base station, and we assume  $r \ll d$ . The users are assumed to be uniformly distributed within the circular area. In general, a network might consist of several such clusters, but here we focus on one, assuming that the other clusters are geographically far.

We assume that the downlink channel vector of user  $i$  at time  $t$  is modeled by<sup>8</sup>

$$\mathbf{h}_i(t) = \sqrt{\rho} \sum_{k=1}^P \alpha_{i,k}(t) \mathbf{e}(\theta_{i,k}(t)),$$

where  $\rho$  is the path loss factor (assumed constant across users in the same cluster since  $r \ll d$ ),  $P$  is the number of signal paths,  $\alpha_{i,k}(t) \sim \mathcal{CN}(0, 1)$  is the complex path gain for the  $k$ th path of user  $i$  at time  $t$ ,  $\theta_{i,k}$  is the angle of departure of the  $k$ th path of the  $i$ th user at time  $t$ , and  $\mathbf{e}(\theta)$  is given by

$$\mathbf{e}(\theta) := \begin{bmatrix} 1 & e^{j2\pi\Delta \cos(\theta)} & e^{j2\pi2\Delta \cos(\theta)} & \dots & e^{j2\pi(M-1)\Delta \cos(\theta)} \end{bmatrix}^*,$$

<sup>8</sup>This is written for a uniform linear transmit array for simplicity, but our analysis using this model can be generalized for any array configuration.

for an antenna separation  $\Delta$ . The path gains  $\alpha_{i,k}(t)$  are i.i.d. across different  $i$ ,  $k$ , and  $t$ .

Path loss between users is modeled by  $\phi_{ij} = \phi_0 d_{ij}^\alpha$  for some constant  $\phi_0$ , where  $d_{ij}$  is the distance between  $i$  and  $j$ , and  $\alpha > 2$  is the path loss exponent.

For simplicity of analysis, in this example network we will assume that only one cooperative pair per time slot is scheduled. Our goal is to characterize the cooperation gains in SNR when one is allowed to choose the most suitable relay  $j$  for a given destination  $i$ .

Invoking (6), we define the cooperative SNR for the pair  $(i, j)$ ,  $\text{SNR}_{ij}^{\text{coop}}$  to be

$$\text{SNR}_{ij}^{\text{coop}} := \frac{s_{ij1}^2}{1 + |u_{ijk}(2)|^2 \frac{\sigma_{ji}^2}{2^{R_{ij}-1}}},$$

where  $s_{ij1}$  is the first singular value corresponding to the pair  $(i, j)$ . Since we are interested in the achievable SNR gain, in defining this quantity, we have allocated all power to only one of the available streams, ignoring the multiplexing gain that could be achieved by scheduling two parallel streams to user  $i$ . The maximal non-cooperative SNR for user  $i$  is given by  $\text{SNR}_i^{\text{non-coop}} := \|\mathbf{h}_i\|^2$ , achieved by beamforming along the direction of  $h_i$ . Minimum cooperative and non-cooperative SNRs in the network are respectively defined as

$$\text{SNR}_{\min}^{\text{coop}} := \min_{i \in \mathcal{N}} \text{SNR}_{ij^*(i)}^{\text{coop}}, \quad \text{SNR}_{\min}^{\text{non-coop}} := \min_{i \in \mathcal{N}} \text{SNR}_i^{\text{non-coop}},$$

where  $j^*(i) = \arg \max_{j \in \mathcal{N}} \mathbb{E} [\text{SNR}_{ij}^{\text{coop}} | \phi_{ij}, \mathbf{h}_j]$ , which arises due to relay selection, and the expectation is taken over the D2D side-channel fading  $\nu_{ij}(t)$ .

The next theorem, whose proof is in Appendix A, summarizes our results on how the SNR of the weakest user in either case scales with the number of users  $n$  in the cluster.

**Theorem 4.**

$$\lim_{n \rightarrow \infty} \mathbb{P} \left( \text{SNR}_{\min}^{\text{coop}} < \frac{1}{2} M \rho \left( \frac{1}{2} \log n - 2 \log \log n \right) - 1 \right) = O \left( e^{-\log^2 n + 2 \log n} \right),$$

and

$$\lim_{m \rightarrow \infty} \mathbb{P} \left( \text{SNR}_{\min}^{\text{non-coop}} > M \rho n^{-\frac{\gamma}{2P}} g(2P) \right) = O \left( e^{-n^{1-\gamma}} \right),$$

for any  $0 < \gamma < 1$ , where  $g(\ell) = (\ell!)^{\frac{1}{\ell}}$ , and  $P$  is the number of signal paths.

Theorem 4 highlights the importance of having multiple options in relay selection. In the non-cooperative case, the factor  $n^{-\frac{\gamma}{2P}}$  appears due to the fact that as the number of users in the cluster grows, the minimum is taken over a larger set of users, and hence it is expected for the SNR of the weakest user to decay, in the absence of cooperation. On the other hand,

in the presence of cooperation, the SNR of the weakest user actually *grows*. This is due to the *multiuser diversity gain*, which is present due to our ability to schedule the user with the most favorable channel conditions as a relay. In other words, as the number of users grows, so does the number of possible paths from the base station to each user, and thus the maximal SNR.

#### IV. DOWNLINK SCHEDULING WITH COOPERATION

Although our analysis of the SNR gain with relay selection in the previous section is informative of the potential gains of cooperation, one should note that its scope is limited. In the analysis, we have restricted ourselves to the scheduling of a single flow, and a specific network model. Further, in a real system one may need to guarantee some notion of fairness that considers relaying cost, and ensure the stability of the relay queues. For a more thorough understanding of how to perform relay selection, we embed relay selection into a constrained downlink scheduling problem. We formulate and analyze this problem in this section within the network utility maximization framework [9], [23].

##### A. Utility Maximization Formulation

Utility maximization framework has been extensively studied in the context of resource allocation and scheduling problems for wireless/wired networks [9], [23]. In such problems, the goal is to develop a dynamic resource allocation policy that in the long-term maximizes a concave, non-decreasing “utility” function of the throughputs of each message flow. It is known that various choices of utility function lead to different notions of fairness across the network [24]. We formulate the joint relay selection and scheduling problem within this framework.

In order to account for the relaying cost, we incorporate the fraction of time user  $i$  has performed relaying for other users,  $\beta_i$  (as defined in Section II, Table I), into the utility objective. This naturally introduces a penalty each time a D2D link is scheduled, and thus the out-of-band resources are not “free”. More formally, let  $U_i : [0, \infty) \times [0, 1] \rightarrow \mathbb{R}$ ,  $i \in \mathcal{N}$ , be a twice continuously differentiable concave utility function that is non-decreasing in the first argument, and non-increasing in the second argument. The function  $U_i$  represents the network-level “reward” corresponding to user  $i$ , where the first argument represents the long-term average throughput of the user (corresponding to variable  $r_i$ ), and the second one represents the fraction of time user  $i$  has performed relaying for other users in the network, (corresponding to variable  $\beta_i$ ). Note that such a utility function  $U_i(r_i, \beta_i)$  jointly captures the reward of having received an average throughput of  $r_i$ , and the cost of having relayed  $\beta_i$  fraction of time, for user  $i$ . We



will consider a specific form of utility function in Section IV-C, and demonstrate its properties in terms of fairness and relaying cost.

We assume the network state is represented by the pair  $(K(t), L(t))$ , where  $K(t) = (H(t), \Phi)$  corresponds to the component of the network parameters that are causally known at the base station, and  $L(t) = (N(t), B(t))$  corresponds to the components that are unknown. We assume that  $K(t)$  and  $L(t)$  take values over the arbitrarily large but finite sets  $\mathcal{K}$  and  $\mathcal{L}$ , respectively<sup>9</sup>. Define

$$y_{sk\ell}^\pi(t) = \frac{1}{t} \sum_{\tau=1}^t \mathbb{I}_{\mathcal{S}_\pi(\tau)=s} \mathbb{I}_{K(\tau)=k} \mathbb{I}_{L(\tau)=\ell},$$

for  $s \subseteq \mathcal{N}^2 \times \{1, 2\}$ ,  $k \in \mathcal{K}$ , and  $\ell \in \mathcal{L}$ , where  $\mathcal{S}_\pi(t)$  is the active set at time  $t$  under policy  $\pi$  and  $\mathbb{I}_C$  is the indicator variable for the event  $C$ ; *i.e.*,  $y_{sk\ell}^\pi(t)$  is the average fraction of time the network was in state  $(k, \ell)$ , and the policy  $\pi$  chose the active set  $s$  up to time  $t$ .

Under this definition, our joint scheduling/relay selection problem can be formulated as the following utility optimization problem.

$$\text{maximize } \sum_{i \in \mathcal{N}} U_i(r_i, \beta_i) \quad \text{s.t. } (\mathbf{r}, \beta) \in \mathcal{R}, \quad \beta \in \Lambda, \quad (7)$$

where  $\mathcal{R}$  is such that  $(\mathbf{r}, \beta) \in \mathcal{R}$  if and only if there exists a scheduling policy  $\pi$  such that

$$\liminf_{t \rightarrow \infty} \sum_{s: i \in s_1} \sum_{k \in \mathcal{K}} \sum_{\ell \in \mathcal{L}} R_{sk\ell}^{(i)} y_{sk\ell}^\pi(t) = r_i, \quad \limsup_{t \rightarrow \infty} \sum_{s: i \in s_2} \sum_{k \in \mathcal{K}} \sum_{\ell \in \mathcal{L}} y_{sk\ell}^\pi(t) = \beta_i$$

almost surely for all  $i \in \mathcal{N}$ , where  $s_1 := \{i : (i, j, k) \in s\}$ ,  $s_2 := \{j : (i, j, k) \in s, i \neq j\}$ , and  $R_{sk\ell}^{(i)}$  is the rate delivered to user  $i$  when  $\mathcal{S}_\pi = s, \mathcal{K} = k, \mathcal{L} = \ell$ , which can be computed based on the results from Section III. Note that in the optimization problem (7), the first constraint simply ensures feasibility of the pair  $(\mathbf{r}, \beta)$ , and the second one imposes the stability constraint for the relay queues, given the conflict graph  $\mathcal{G}_c$  between the flows  $(i, j)$  available in the network.

## B. Optimal Scheduling

Note that due to interference (conflicts) between D2D links, not all D2D users can transmit at the same time, which implicitly imposes a constraint on downlink scheduling in order to keep the relay queues stable. The existing cross-layer design tools [9], [23] (e.g., virtual queues, dynamic

<sup>9</sup>The finiteness assumption is made for technical convenience in proofs; however the proposed scheduling algorithm itself does not rely on this assumption. By assuming a large cardinality, one can model the general case with uncountable alphabets arbitrarily closely.

backpressure routing etc.) do not immediately extend to our cooperative downlink model when D2D transmission conflicts are taken into account. This is firstly because our physical layer signaling is not based on routing, and makes explicit use of the broadcast nature of the wireless medium, by using both the direct link to the destination node, and the alternate link formed by relay. Consequently, the full network cannot be abstracted into a graph with isolated links, which is widely assumed in the literature<sup>10</sup>. Secondly, since our utility metric is a function of the average amount of relaying done by users, the network-level objective also depends on *how* the information is delivered, since different choices of relay for the same user results in different rewards, even when the rates offered in these choices are equal. The existing formulations within network utility maximization framework does not capture this generalization, since the routing decisions are essentially decoupled from which utility objective is being employed. Hence, we need a special treatment of the downlink resource allocation problem with D2D cooperation.

To achieve this, we take an approach consisting of

- 1) A generalization of the single-user scheduling algorithm of [1] based on the maximization of the derivative of the utility function to the cooperative scenario with relay selection, MU-MIMO, and incomplete network state knowledge,
- 2) A novel relay flow control scheme integrated into scheduling, which involves an explicit characterization of an inner bound on the system stability region in terms of a set linear constraints on the arrival rates, and imposing these hard constraints in relay selection,
- 3) A novel utility metric that is specific to the cooperative architecture, exhibiting desirable fairness properties.

In particular, the second point requires the use of a novel technique using exponential barrier functions to handle the stability constraint, and the generalizations of the first point requires several modifications to the proof of [1].

We will next characterize the inner bound on the stability region for the relay queues subject to the constraints imposed by the conflict graph  $\mathcal{G}_c$ .

*1) Stability region structure:* We consider the set of relay queues  $Q_{ij}$ ,  $i \neq j$ , subject to the simultaneous transmission constraints represented by  $\mathcal{G}_c$ . Since this system constitutes a one-hop network, depending on the conflict graph structure, the stability region may be expressed explicitly in terms of linear constraints on arrival rates. If it cannot, then one can always back

<sup>10</sup>In non-cooperative MU-MIMO downlink scheduling problem (e.g., [8]), the network can be abstracted into a graph assuming beamforming and treating inter-beam interference as noise; however once cooperation is enabled the explicit use of the coupling between different user outputs prevent such an abstraction.

off from the optimal stability region by iteratively adding edges to the conflict graph until the resulting graph admits an explicit characterization of stability region.

The results in [12] can be used to show that the stability region of the constrained queueing network formed by the  $n$  users is given by

$$\Lambda = \{ \beta : \mathbf{D}^{-1} \beta \in \text{conv}(\Pi) \}, \quad (8)$$

where  $\mathbf{D}$  is a diagonal matrix with  $p_{ij}$  values on the diagonal ( $p_{ij} > 0$  without loss of generality),  $\text{conv}(\cdot)$  represents the convex hull of a set of vectors, and  $\Pi$  is the set of incidence vectors of the independent sets of  $\mathcal{G}_c$ , i.e., a vector  $\mathbf{s}$  whose elements are indexed by  $(i, j)$  is contained in  $\Pi$  if  $\{(i, j) : s_{(i,j)} = 1\}$  is an independent set of  $\mathcal{G}_c$ <sup>11</sup>.

The set  $\Lambda$  as defined in (8) is known as the stable set polytope of the graph  $\mathcal{G}_c$ . The exact characterization of  $\Lambda$  is not known in general [25], although several outer bounds are known, which are tight for certain classes of graphs (see [25] for more on the characterization of stable set polytopes). Here, we will focus on the most well-known class among these, known as *perfect graphs*. A graph  $\mathcal{G}$  is *perfect* if its chromatic number  $\chi(\mathcal{G})$  is equal to its maximum clique size  $\omega(\mathcal{G})$ . A *maximal clique* of a graph  $\mathcal{G} = (\mathcal{V}, \mathcal{E})$  is a subset of vertices  $\mathcal{A} \subseteq \mathcal{V}$  that satisfies the clique property, and for any  $u \in \mathcal{V} - \mathcal{A}$ ,  $\{u\} \cup \mathcal{A}$  is not a clique. Stable set polytopes of perfect graphs can be completely described in terms of their maximal cliques, as characterized in the following theorem.

**Theorem 5.** [26] *Let  $\mathcal{Q}$  be the set of maximal cliques of a perfect graph  $\mathcal{G}$ . Then the stable set polytope of  $\mathcal{G}$  is the set of vectors  $x \in [0, 1]^{|\mathcal{V}|}$  satisfying  $\sum_{v \in Q} x_v \leq 1$  for all  $Q \in \mathcal{Q}$ .*

Theorem 5 enables us to characterize the stability region of our queueing system in terms of explicit linear constraints on the vector of arrival rates  $\beta$ , provided that the conflict graph is perfect. In general, our construction of conflict graph in (1) does not preclude the possibility of a non-perfect graph, e.g., a graph that contains a chordless odd cycle of size larger than 3. However, one can back off from the optimal stability region by adding new edges to the conflict graph such that the resulting graph is perfect. One example such process is *chordalization*. A graph is *chordal* if, for every cycle of length larger than three, there is an edge that is not part of the cycle, connecting two of the vertices of the cycle. Chordal graphs are known to be perfect, and any graph can be chordalized in polynomial time. Moreover, the maximal cliques

<sup>11</sup>The boundary of the stability region is included in the set  $\Lambda$  for technical convenience. Note that this does not change the supremum value in the optimization (7) since the objective function is continuous.

of a chordal graph can be listed in polynomial time [27], which make them viable candidates for our purposes.

With this back-off, we reformulate the optimization (7) as

$$\text{maximize } \sum_{i \in \mathcal{N}} U_i(r_i, \beta_i) \quad \text{s.t. } (\mathbf{r}, \beta) \in \mathcal{R}, \quad \beta \in \bar{\Lambda}. \quad (9)$$

where  $\bar{\Lambda} \subseteq \Lambda$  denotes the new stability region obtained by inserting edges in  $\mathcal{G}_c$ , such that the corresponding conflict graph  $\bar{\mathcal{G}}_c$  is perfect. Clearly,  $\bar{\Lambda} = \Lambda$  if  $\mathcal{G}_c$  is perfect. The optimality of the proposed scheduling algorithm is with respect to this reduced stability region  $\bar{\Lambda}$ .

2) *An optimal policy:* We now propose a scheduling policy that is asymptotically guaranteed to achieve the optimum of (9). Note that by fixing the physical layer scheme, we effectively restrict ourselves to a class of strategies  $\Gamma$  indexed by  $\mathcal{S} \subseteq \mathcal{N}^2 \times \{1, 2\}$ , and thus the scheduling policy only chooses the subset  $\mathcal{S}$ . Let  $\mathcal{Q}$  be the set of maximal cliques of  $\mathcal{G}_c$ . For  $Q \in \mathcal{Q}$ , we denote  $\beta_Q := \sum_{(i,j) \in Q} \frac{\beta_{ij}}{p_{ij}}$ .

Consider the following policy, which we call  $\pi^*$ : Given  $(\mathbf{r}(t-1), \beta(t-1), H(t), \Phi)$ , choose the subset  $s^*$  of streams such that  $s^* = \arg \max_{s \subseteq \bar{\mathcal{N}}(t) \times \{1, 2\}} f(s)$ , where

$$f(s) = \sum_{(i,j,k) \in s} \mathbb{E}_{L(t)} \left[ R_{sK(t)L(t)}^{(i)} \middle| K(t) \right] \frac{\partial U_i}{\partial r_i} \bigg|_{\substack{r_i=r_i(t-1) \\ \beta_i=\beta_i(t-1)}} + \frac{\partial U_j}{\partial \beta_j} \bigg|_{\substack{r_j=r_j(t-1) \\ \beta_j=\beta_j(t-1)}}, \quad (10)$$

$\bar{\mathcal{N}}(t) := \{(i, j) \in \mathcal{N}^2 : \beta_Q \leq 1 \text{ for all } Q \in \mathcal{Q} \text{ s.t. } (i, j) \in Q\}$ . Note that  $(i, i) \in \bar{\mathcal{N}}(t)$  is vacuously true for all  $i$ , corresponding to the scenario where user  $i$  is scheduled without relay.

Note that since the maximization in the scheduling rule is over a superset of the set of all possible non-cooperative schedule sets, the cooperative architecture cannot result in a lower utility than the non-cooperative one, and thus always results in a gain with respect to the non-cooperative architecture.

**Theorem 6.** *Let the optimal value of the maximization in (9) be OPT. Define the empirical utility of  $\pi^*$  as  $U^*(t) = \sum_{i \in \mathcal{N}} U_i(r_i^*(t), \beta^*(t))$ , where  $r_i^*(t)$  is the average throughput of user  $i$  up to time  $t$ , and  $\beta^*(t)$  is the fraction of time user  $i$  has spent relaying for other users up to time  $t$ , under the policy  $\pi^*$ . Then the following holds:*

- 1)  $\lim_{t \rightarrow \infty} \inf \{ \|\beta^*(t) - \beta\|_1 : \beta \in \bar{\Lambda} \} = 0$  almost surely,
- 2)  $\lim_{t \rightarrow \infty} U^*(t) = \text{OPT}$  almost surely.

The proof outline is provided in Section IV-D, with details in Appendix B. Theorem 6 shows that policy  $\pi^*$  asymptotically achieves the optimum of (9). There are a few key points to note in the definition of policy  $\pi^*$ . First, note that the maximization is performed over the available

streams  $(i, j, k)$  in the network, as opposed to over the set of users themselves. Second, at any time slot  $t$ , any stream  $(i, j, k)$  that involves a pair of users  $(i, j)$  that is part of a clique  $Q$  that currently violates its constraint  $\beta_Q \leq 1$  is ignored in the maximization, which is the relay flow control component of the algorithm to ensure stability of the relay queues. Third, the asymptotic optimality of  $\pi^*$  reveals that it is sufficient to average the rate  $R_{sKL}^{(i)}$  over the part of the network state  $L(t)$  that is unknown at the base station, which is consistent with the results in [8]. Finally, since our utility function involves the relaying cost as well as throughputs, the scheduling law involves partial derivatives with respect to both of these variables.

### C. Choice of Utility Function

We focus on utility functions of the form

$$U_i(r_i, \beta_i) = u_i(r_i) + v_i(1 - \beta_i), \quad (11)$$

where  $u_i$  and  $v_i$  are twice continuously differentiable, non-decreasing, concave functions that capture fairness in throughput, and fairness in relaying load, respectively. Specific choices of  $u_i$  and  $v_i$  in (11) may lead to different notions of fairness. We will be particularly interested in the case where  $u_i(x) = \log(x)$  and  $v_i(x) = C \log(x)$ , where<sup>12</sup>  $C$  is a parameter that controls the trade-off between fairness in throughput and fairness in relaying load. Clearly,  $C = 0$  corresponds to the well-known *proportional fairness* [24]. For an arbitrary  $C$ , let  $(\tilde{\mathbf{r}}, \tilde{\beta})$  solve the optimization (9) with  $U_i(r_i, \beta_i) = \log(r_i) + \log(1 - \beta_i)$ , where

$$r_i = \sum_{s:i \in s_1} \sum_{k \in \mathcal{K}} \sum_{\ell \in \mathcal{L}} R_{skl}^{(i)} y_{skl}, \quad \beta_i = \sum_{s:i \in s_2} \sum_{k \in \mathcal{K}} \sum_{\ell \in \mathcal{L}} y_{skl}.$$

Note that here  $y_{skl}$  has no time dependence and refers to a deterministic quantity, *i.e.*, the fraction of time for which  $\mathcal{S}(t) = s, K(t) = k, L(t) = \ell$ , throughout the (infinite) duration of transmission. Then, for any feasible perturbation  $\delta \mathbf{y}$  that pushes the operating point from  $(\tilde{\mathbf{r}}, \tilde{\beta})$  to  $(\mathbf{r}, \beta)$ , it must be that  $\sum_{s,k,\ell} \delta y_{skl} \sum_i \frac{\partial U_i}{\partial y_{skl}} \leq 0$  by concavity, which, using the facts

$$r_i - \tilde{r}_i = \delta r_i = \sum_{s:i \in s_1} \sum_{(k,\ell) \in \mathcal{K} \times \mathcal{L}} R_{skl}^{(i)} \delta y_{skl}, \quad \beta_i - \tilde{\beta}_i = \delta \beta_i = \sum_{s:i \in s_2} \sum_{(k,\ell) \in \mathcal{K} \times \mathcal{L}} \delta y_{skl}$$

can be re-arranged into

$$\sum_i \frac{r_i - \tilde{r}_i}{\tilde{r}_i} \leq C \sum_i \frac{(1 - \tilde{\beta}_i) - (1 - \beta_i)}{1 - \tilde{\beta}_i}. \quad (12)$$

<sup>12</sup>Note that this choice means that the function is not defined for  $\beta_i = 1$  and  $r_i = 0$ , but we ignore this since no user will operate at these points.

The condition (12) admits a meaningful interpretation. Note that the left-hand side represents the sum of the relative gains in throughput due to the perturbation, whereas the right hand-side represents the sum of the relative decrease in time spent non-relaying. The condition in (12) then suggests that any perturbation to the optimal values will result in a total percentage throughput gain that is less than the total percentage increase in relaying cost, with the parameter  $C$  acting as a translation factor between throughput and relaying cost. This can be considered a generalization of well-studied proportional fairness, which implies that any perturbation to the optimal operating point results in a total percentage throughput loss. Our generalization allows for a positive total relative throughput change, albeit only at the expense of a larger total relative cost increase in relaying. For this utility function, we can evaluate the scheduling rule (10) as

$$s^* = \arg \max_{s \subseteq \mathcal{N}(t) \times \{1,2\}} \frac{\mathbb{E}_{L(t)} \left[ R_{sK(t)L(t)}^{(i)} \middle| K(t) \right]}{r_i(t)} - \frac{C}{1 - \beta_{ij}(t)}.$$

#### D. Proof Outline of Theorem 6

In this section, we provide the proof outline of Theorem 6, leaving details to Appendix B.

We begin with the first claim of Theorem 6. Due to Theorem 5, it is sufficient to show that for any maximal clique  $Q \subseteq \mathcal{V}_c$ ,  $\limsup \beta_Q^*(t) \leq 1$  almost surely. Assume that there exists  $\epsilon > 0$ ,  $Q \in \mathcal{Q}$ , such that for any  $N$ , there exists  $t > N$  that satisfies  $\beta_Q^*(t) > 1 + \epsilon$ . Note that

$$\beta_Q^*(t) \leq \frac{t-1}{t} \beta_Q^*(t-1) + \frac{|Q|}{tp} \mathbb{I}_{\beta_Q^*(t-1) < 1}, \quad (13)$$

with  $p = \min_{(i,j) \in Q} p_{ij}$ , where the upper bound is obtained by observing that the maximal increase in  $\beta_Q^*(t)$  is achieved when all flows  $(i, j) \in Q$  are scheduled at slot  $t$ . Choosing  $N = \frac{|Q|}{\epsilon p}$ , there must exist  $t > N$  s.t.  $\beta_Q^*(t) > 1 + \epsilon$ . Letting  $t^* \geq N$  to be the smallest of such indices, it must be that  $\beta_Q^*(t^* - 1) \leq 1$ , since otherwise the increment  $\beta_Q^*(t) - \beta_Q^*(t-1)$  cannot be positive, by construction. But by (13) and by the choice of  $N$ ,

$$\beta_Q^*(t^*) \leq \frac{t^* - 1}{t^*} \beta_Q^*(t^* - 1) + \epsilon \mathbb{I}_{\beta_Q^*(t^*-1) < 1} \leq 1 + \epsilon,$$

which is a contradiction. This proves the first claim, and establishes the feasibility of  $(\mathbf{r}^*, \beta^*)$ .

The proof of the second claim uses stochastic approximation techniques similar to the main proof in [1], but also features several key differences to account for D2D cooperation, multiuser MIMO, partial network knowledge, relay queue stability, and generalized utility functions. To prove the second claim, we first reformulate (9) in terms of the variables  $y_{sk\ell}$ , as follows

$$\text{maximize } U(\mathbf{y}) := \sum_{i \in \mathcal{N}} U_i \left( \sum_{s:i \in s_1} \sum_{k \in \mathcal{K}} \sum_{\ell \in \mathcal{L}} R_{sk\ell}^{(i)} y_{sk\ell}, \sum_{s:i \in s_2} \sum_{k \in \mathcal{K}} \sum_{\ell \in \mathcal{L}} y_{sk\ell} \right) \quad (14)$$

$$\text{s.t. } y_{sk\ell} \geq 0, \quad \sum_s y_{sk\ell} \leq p_k q_\ell, \quad y_{sk\ell} = q_\ell \sum_{\ell'} y_{sk\ell'}, \quad \forall s, k, \ell \quad (15)$$

$$\sum_{(i,j) \in Q} \sum_{\substack{s: i \in s_1 \\ j \in s_2}} \sum_{k \in \mathcal{K}} \sum_{\ell \in \mathcal{L}} y_{sk\ell} \leq 1, \quad \forall Q \in \mathcal{Q}, \quad (16)$$

where  $p_k = \mathbb{P}(K(t) = k)$ , and  $q_\ell = \mathbb{P}(L(t) = \ell)$ , where  $y_{sk\ell}$  are deterministic; they represent the fraction of time spent in state  $(s, k, \ell)$  throughout the transmission. The last condition in (15) reflects the fact that the scheduling decision cannot depend on the realization of  $L(t)$ , since this information is not available at the base station.

**Lemma 1.** *Let  $\text{OPT}'$  denote the optimal value of (14). Then  $\text{OPT}' \geq \text{OPT}$ .*

*Proof:* For any  $n \in \mathbb{N}$ , let  $\pi_n$  be a feasible policy such that  $\liminf_{t \rightarrow \infty} U^{\pi_n}(t) \geq \text{OPT} - \frac{1}{2n}$ . Then by definition, there must exist  $T_n$  such that for  $t > T_n$ ,  $U^{\pi_n}(t) \geq \text{OPT} - \frac{1}{n}$ . Consider the sequence  $\mathbf{y}^{\pi_n}(T_n)$ , where  $U^{\pi_n}(t) = U(\mathbf{y}^{\pi_n}(t))$ . Let the set of vectors  $\mathbf{y}$  defined by (15) and (16) be  $\mathcal{Y}$ . Then strong law of large numbers, and the independence of  $(\mathcal{S}(t), K(t))$  from  $L(t)$  implies  $\lim_{n \rightarrow \infty} \inf \{ \|\mathbf{y} - \mathbf{y}^{\pi_n}(T_n)\| : \mathbf{y} \in \mathcal{Y} \} = 0$ . Therefore, there exists a sequence  $\{\mathbf{y}_n\} \in \mathcal{Y}$  such that  $\lim_{n \rightarrow \infty} \|\mathbf{y}_n - \mathbf{y}^{\pi_n}(T_n)\| = 0$ . Since  $\mathcal{Y}$  is closed and bounded, it is compact, and therefore  $\mathbf{y}_n$  must have a subsequence, say  $\mathbf{y}_{n_k}$ , that converges to a point  $\mathbf{y}^* \in \mathcal{Y}$ , which implies  $\lim_{k \rightarrow \infty} \mathbf{y}^{\pi_{n_k}}(T_{n_k}) = \mathbf{y}^* \in \mathcal{Y}$ . Since the function  $U$  is continuous, we have

$$\text{OPT} = \lim_{k \rightarrow \infty} U(\mathbf{y}^{\pi_{n_k}}(T_{n_k})) = U\left(\lim_{k \rightarrow \infty} \mathbf{y}^{\pi_{n_k}}(T_{n_k})\right) = U(\mathbf{y}^*).$$

Since  $\mathbf{y}^*$  is in the feasible set  $\mathcal{Y}$ , it must be that  $\text{OPT}' \geq U(\mathbf{y}^*) = \text{OPT}$ .  $\blacksquare$

Using Lemma 1, it is sufficient to show that  $U^*(t)$  converges to the optimum value of (14). We state this in the following lemma, whose proof is provided in Appendix B.

**Lemma 2.**  $\lim_{t \rightarrow \infty} U^*(t) = \text{OPT}'$ , *almost surely.*

The proof of Lemma 2 extends the stochastic approximation techniques from [1], [2] to our setup, using a sequence of exponential barrier functions to handle the stability constraint.

### E. Greedy Scheduling

Although converging to the optimal solution, the policy  $\pi^*$  suffers from high computational complexity, since it involves an exhaustive search over all subsets of streams. To reduce the complexity, we consider a greedy implementation of the policy, similar to [3] for non-cooperative MU-MIMO. Although the greedy algorithm is suboptimal in general, it greatly reduces the computational load, and performs well in simulations under reasonably realistic channel models.

The algorithm works by iteratively building the schedule set, at each step adding the stream  $(i^*, j^*, k^*)$  that contributes the largest amount to the objective  $f(s)$ , and committing to this choice in the following iterations, until there are no streams left that can result in a positive utility increment to the existing schedule set. The pseudocode is given in Algorithm 1. Note that in the

---

**Algorithm 1** Greedy cooperative scheduling
 

---

```

1:  $iter = 1, schedule\_set = \emptyset$ 
2: while  $iter \leq max\_streams$  do
3:    $(i^*, j^*, k^*) = \arg \max_{(i,j,k) \in \mathcal{N}(t) \times \{1,2\}} f(schedule\_set \cup (i, j, k))$ 
4:    $f^*(iter) = f(schedule\_set \cup (i^*, j^*, k^*))$ 
5:   if  $f^*(iter) > f^*(iter - 1)$  then
6:      $schedule\_set = schedule\_set \cup (i^*, j^*, k^*)$ 
7:      $iter = iter + 1$ 
8:   else
9:     for all  $Q \in \mathcal{Q}$  do
10:       $\beta_Q(t+1) = update\_clique\_states(\beta_Q(t), schedule\_set)$ 
11:    end for
12:    stop
13:   end if
14: end while

```

---

maximization in line 3, one only needs to consider the neighbors of each user in  $\mathcal{G}$ . Therefore, if the maximum node degree in  $\mathcal{G}$  is  $d$ , then the maximization has worst-case complexity  $O(nd)$ , and thus the scheduling part of the algorithm has worst-case complexity  $O(Nnd)$ , where  $N$  is the maximum number of streams that can be scheduled at a time. Once the scheduling is done,  $\beta_Q$  values are updated using the *update\_clique\_states* subroutine. Since  $\mathcal{G}_c$  is chordal, the number of maximal cliques is bounded by  $n^2$  [28], hence the worst-case complexity of the clique updates is  $O(Nn^2)$ . In practice, the number of users that can be simultaneously scheduled is significantly fewer than both the number of antennas and the total number of users, hence  $N$  is typically not very large (see simulations for its empirical CDF).

## V. SIMULATION RESULTS

We performed system-level simulations of a multi-cell network to characterize the gains of the proposed cooperative architecture.

### A. Simulation Setup

1) *Geographic distribution*: Our simulation setup consists of a hexagonal grid of  $N_c$  cells, each of radius  $R_c$ , with a base station at the center, and  $N_u$  users at each cell. For each cell, we



TABLE II: System parameters used in the simulations

Parameter	Value	Parameter	Value
Cellular bandwidth	40MHz	Cellular carrier freq.	2GHz
D2D bandwidth	40MHz	Side-channel carrier freq.	5GHz
# BS antennas	32 (linear array)	OFDM FFT size	2048
# UE antennas	1 cell.+1 ISM	Power allocation	equal
Antenna spacing	$0.5\lambda$	BS power	46dBm
BS antenna gain	0 dBi	UE power	23dBm
BS antenna pattern	Uniform	Penetration loss	0dB

TABLE III: Default cell-size-specific parameters

	Large Cell	Small Cell
<b>Inter-site distance</b> ( $R_c\sqrt{3}$ )	1732m	500m
<b>No. cells</b> ( $N_c$ )	5	19
<b>No. active users/cell</b> ( $N_u$ )	25	10
<b>Cluster radius std. dev.</b> ( $\sigma$ )	20m	10m
<b>Mean no. clusters</b> ( $\frac{3\sqrt{3}}{2}\lambda R_c$ )	5	3
<b>Utility trade-off param.</b> ( $C$ )	7	8

first generate a set of cluster centers according to a homogeneous Poisson point process with density  $\lambda$ . Next, we randomly assign each user to a cluster, where each user location vector  $\mathbf{x}$  for cluster  $i$  is randomly chosen i.i.d. according to  $\mathbf{x} \sim \mathcal{CN}(\mathbf{c}_i, \sigma^2 \mathbf{I}_2)$ , where  $\mathbf{c}_i$  is the  $i$ 'th cluster center, with  $\sigma$  determining how localized versus dispersed the cluster is. For each set of spatial parameters, we generate eight ‘‘drops’’, *i.e.*, instantiations of user distributions, and the CDFs are computed through aggregating the results across the drops.

2) *Channel model*: For each (BS, user) pair, we generate a time series of 100 channel vectors for each OFDM subcarrier using the 3GPP Spatial Channel Model (SCM) implementation [29], assuming a user mobility of 3m/s. For each user pair in a cell, we use the models from 3GPP D2D Channel Model [30] to generate the path loss parameter  $\phi_{ij}$  and the log-normal shadowing parameter  $\xi_{ij}$ . The channel between the user pair  $(i, j)$  for each resource block is then computed as  $\phi_{ij}\xi_{ij}\nu_{ij}$ , where  $\nu_{ij} \sim \mathcal{CN}(0, 1)$  is i.i.d. fading parameter for a given resource block. The fading parameters are assumed to be independent across resource blocks for simplicity. For the main results, we use the line-of-sight (LOS) model, but we also explore the effect of non-line-of-sight links later in the section. For each drop, the channels are computed in this way and stored *a priori*, and all the simulations are run for the same sequences of channel realizations.

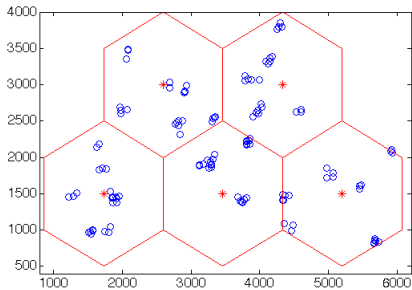


Fig. 3: Sample geographic distribution of users for large cells.

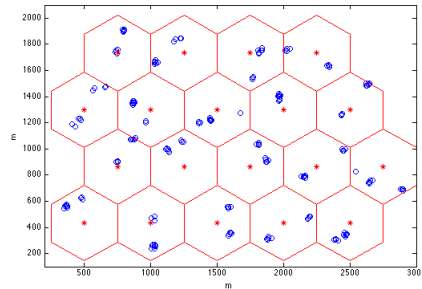


Fig. 4: Sample geographic distribution of users for small cells.

3) *System operation:* Various system parameters are given in Table II. We assume that at every time slot, the base station obtains an estimate of the current network state (estimation error modeled as a Gaussian random variable with variance proportional to the total energy of the channel gains across the OFDM subcarriers, independently for each antenna), and makes a scheduling decision. The scheduling decision is made without knowledge of the inter-cell interference. In the cooperative case, scheduling is done according to Algorithm 1. In the non-cooperative case, Algorithm 1 is used with the maximization in line 3 done over the set  $\{(i, i, 1) : i \in \mathcal{N}\}$ , and clique states are not updated since there are no cliques. Note that this reduces to the greedy scheduling algorithm of [3]. Once the scheduling decision is made, the throughput is computed using the results of Section III based on the actual channel realizations with inter-cell interference, and a 3dB SNR back-off to model practical coding performance. We also take into account various rate back-offs including OFDM cyclic prefix and guard intervals, channel training and uplink data bursts. When a user is scheduled, the whole cellular bandwidth is used for transmission to that user, *i.e.*, users are multiplexed spatially (through zero-forcing beamforming with regularization), not spectrally. After the transmission, user throughputs and relaying fractions are updated through

$$r_i(t+1) = \left(1 - \frac{1}{T_w}\right) r_i(t) + \frac{1}{T_w} R_i(t),$$

$$\beta_i(t+1) = \left(1 - \frac{1}{T_w}\right) \beta_i(t) + \frac{1}{T_w} |\{(m, i, k) \in \mathcal{S}(t) : m \in \mathcal{N} - \{i\}, k \in \{1, 2\}\}|,$$

where  $R_i(t)$  is the rate delivered to user  $i$  at time  $t$ , and  $T_w$  is the averaging window (used  $T_w = 50$  in simulations).

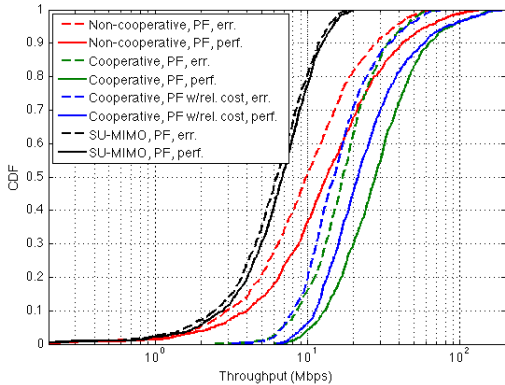


Fig. 5: Throughput CDF for large cells.

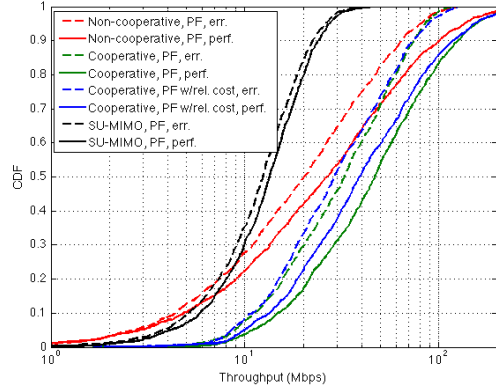


Fig. 6: Throughput CDF for small cells.

### B. Throughput Distribution

For the setup described in the previous subsection, we simulate the system with and without cooperation, under the utility function introduced in Section IV, as well as conventional proportionally fair (PF) scheduler. We consider large and small cells, with parameters corresponding to either case provided in Fig. III. For each case, we simulate the system with and without channel estimation errors, using  $p_{ij} = 1$  for all  $(i, j)$  (we explore smaller values of  $p_{ij}$  later in the section).

The CDF of the long-term average throughput received by the users in the network is plotted in Figures 5 and 6 (“err.” represents the case with channel estimation errors, and “perf.” represents perfect channel estimation). These plots can be interpreted as a cumulative throughput histogram in the network, where the value on the vertical axis represents the fraction of users who experience a throughput that is less than or equal to the corresponding value on the horizontal axis.

One can observe from Figures 5 and 6 that, cooperation is most helpful for the weakest (cell-edge) users in the network, providing a throughput gain ranging from  $3.7\times$  up to  $4.5\times$  for the bottom fifth-percentile of users depending on the channel estimation quality and utility function used, compared to non-cooperative MU-MIMO. The gain for the median user similarly ranges from  $1.5\times$  up to  $2.1\times$  depending on the scenario. The gain gradually diminishes as one considers users with stronger channels, essentially disappearing at the top of the curve.

When the baseline is taken as non-cooperative SU-MIMO, the fifth percentile gain ranges from  $4.3\times$  to  $5.7\times$ , whereas the median gain ranges from  $2.4\times$  up to  $4.1\times$ , where the gain also includes the effect of switching to MU-MIMO.

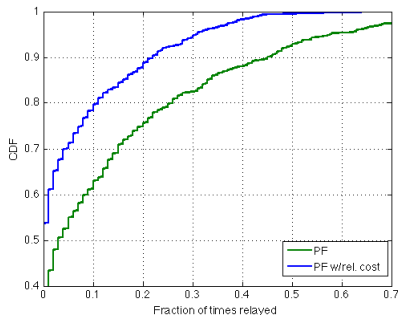


Fig. 7: CDF for the fraction of time spent relaying for large cells.

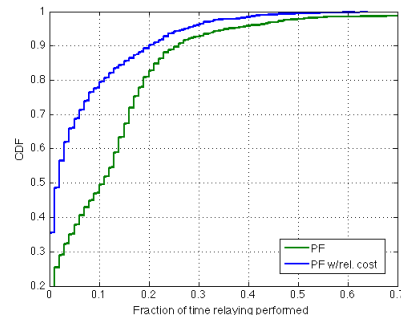


Fig. 8: CDF for the fraction of time spent relaying for small cells.

For the small cell results shown in Figure 6, the gains with respect to non-cooperative MU-MIMO are between  $3\times$  and  $3.8\times$  for the fifth percentile, and between  $1.4\times$  and  $1.8\times$  for the median user. The median user gain from SU-MIMO reaches up to  $3.5\times$  under this scenario.

### C. Relaying Cost

We consider the CDF of the fraction of time a user has performed relaying, for the same runs of simulation as in the previous subsection, for both utility functions, and for the case with channel errors, in Figures 7 and 8. In these figures, the value on the vertical axis represent the fraction of users who perform relaying a fraction of time less than or equal to the corresponding value at the horizontal axis, *e.g.*, 90% of users perform relaying less than 22% of the time for PF with relaying cost, and less than 45% of the time for pure PF utility. We observe that taking the cost of relaying into account in the utility function results in more than 50% drop in the total amount of relaying performed in the network, with a relatively small penalty in throughput. Therefore, the novel utility function proposed in Section IV enables a more efficient utilization of out-of-band resources, from a throughput-per-channel-access perspective. In other words, the proposed utility function results in using D2D relaying only if it gives a large gain in throughput.

### D. Number of Streams Scheduled

We compare the number of streams scheduled per time slot for cooperative and non-cooperative cases, in the CDF in Figures 9 and 10. This can also be understood as the number of steps it takes for Algorithm 1 to terminate.

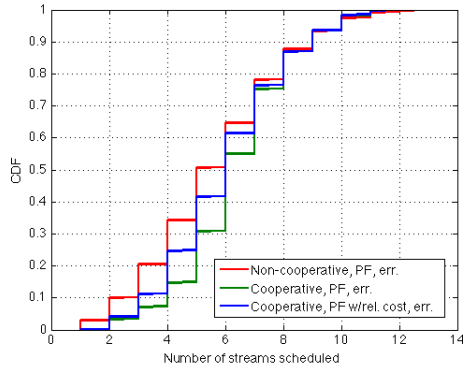


Fig. 9: CDF for the number of streams scheduled for large cells.

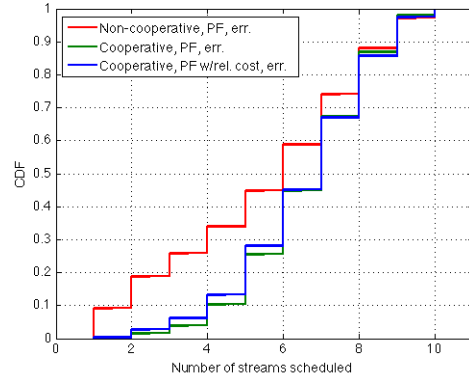


Fig. 10: CDF for the number of streams scheduled for small cells.

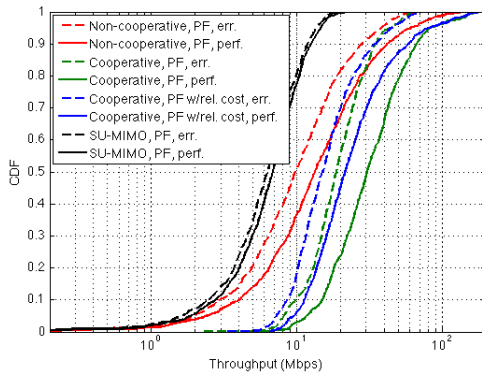


Fig. 11: Throughput CDF for large cells (without stability constraint).

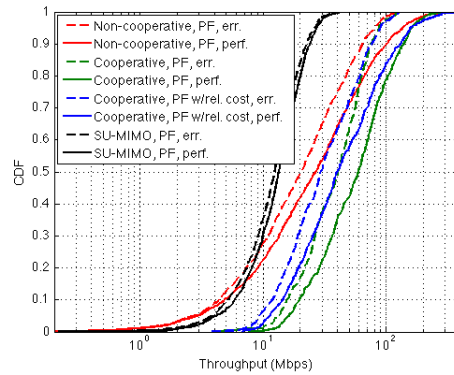


Fig. 12: Throughput CDF for small cells (without stability constraint).

One can observe that cooperation enables the base station to schedule 1-2 additional streams on average, compared to the non-cooperative case. The reason underlying this behavior is the richness in scheduling options, since data can be transmitted to a particular user through several relaying options, with a distinct beamforming vector corresponding to each option. Since it is easier to find a stream (beamforming vector) that is compatible (approximately orthogonal) with the already scheduled streams, on the average the algorithm is able to schedule a larger number of users per time slot.

### E. Relaxing the Stability Constraint

In the scenario where the cellular bandwidth is sufficiently smaller than the D2D bandwidth, the interference constraint no longer active, since the devices can perform frequency-division multiplexing to orthogonalize their transmissions. This scenario can be modeled by removing the stability constraint, and performing the maximization in (10) over all  $\mathcal{N}^2 \times \{1, 2\}$  streams available for scheduling. The resulting throughput CDFs are given in Figures 11 and 12. Comparing the result to those in Figures 5 and 6, we see that the stability constraint has a rather small effect on the cooperative cell-edge gains in throughput for large cells, and a relatively larger effect for small cells. This is because the users are located more densely in small cells, and thus the interference (and thus, the stability) constraint is more restrictive. We observe that under this setup, the fifth-percentile gains with respect to SU-MIMO baseline range from  $3.5\times$  up to  $6.3\times$ , depending on cell size, channel estimation quality and the utility function used. The median gain for large cells reaches almost  $4.5\times$ . The fifth-percentile gains with respect to non-cooperative MU-MIMO are similarly between  $3.3\times$  and  $4.9\times$ , and the median user gain ranges up to  $2.3\times$ .

### F. Effect of Clustering

For large cells, we vary the cluster radius  $R_c$  to study its effect in the throughput CDF in the network. Figure 14 plots the throughputs corresponding to the median and the bottom fifth-percentile users in the network, for a range of cluster radii, cooperative and non-cooperative cases, and line-of-sight (LOS) and non-line-of-sight (NLOS) D2D links. We observe that at 23dBm device power, for LOS links, most of the median and fifth-percentile throughput gains are preserved up to a cluster radius of  $200\text{m}^{13}$ . The decay in throughput is much faster for NLOS D2D links, and the gain completely disappears at a cluster radius of 200m. The performance in a real scenario would be somewhere in between the LOS and NLOS curves, since in a real scenario only a fraction of the links would be LOS.

### G. D2D Link Intermittence

We re-run the simulation in Subsection V-B for smaller values of  $p_{ij}$ . The results are plotted in Figures 13, which suggest that the cell-edge gains are fairly robust to unreliability of the D2D

<sup>13</sup>Note that the cluster radius is the standard deviation of user locations from each cluster center. User pairs with pairwise distance much smaller than the cluster radius can still exist within the cluster.

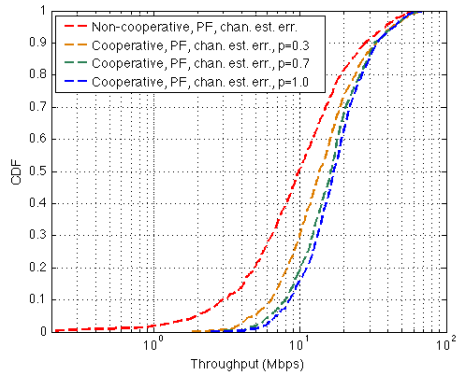


Fig. 13: Throughput CDF for large cells, with intermittent side-channels.

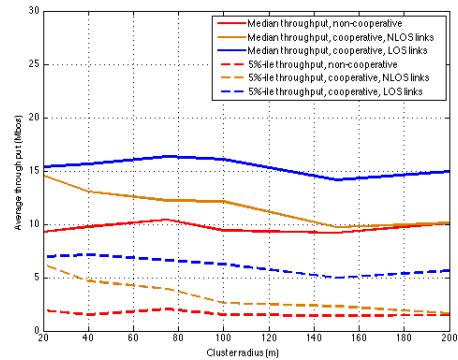


Fig. 14: Median and 5-percentile throughput vs. cluster radius

links, giving approximately  $2.5\times$  gain at the bottom fifth percentile, even when the links are only available 30% of the time.

#### H. Co-existence with WiFi Access Points

Since the existing WiFi and LTE-U networks use the same band as D2D cooperation, an important question is whether co-existence of these technologies negates the possible gains due to interference. In this section, we study this scenario through simulations, and demonstrate that the combined overall benefit of WiFi and D2D strictly dominates the loss due to these transmissions interfering with each other, and thus WiFi and D2D cooperation can co-exist harmoniously.

To study this scenario, we consider a network model where an access point (AP) is placed at each cluster center  $c_i$  (Figure 15). If a user is within the range of a WiFi AP, it only gets served by the AP, and is unavailable for D2D cooperation, since the unlicensed band is occupied by AP transmissions and we assume there is constant downlink traffic from the AP. Otherwise, the user is served by the base station and is potentially available for D2D cooperation. In practice, this co-existence mechanism can be implemented by having the user search for an available channel within the unlicensed band for a specified period of time, to use for D2D cooperation. If none exists, the user can simply declare itself unavailable for D2D cooperation. Note that the D2D transmissions from outside the AP range can still interfere with the receptions of AP users.

We consider a simplified model for the rates delivered by the AP. If there are  $N$  users within

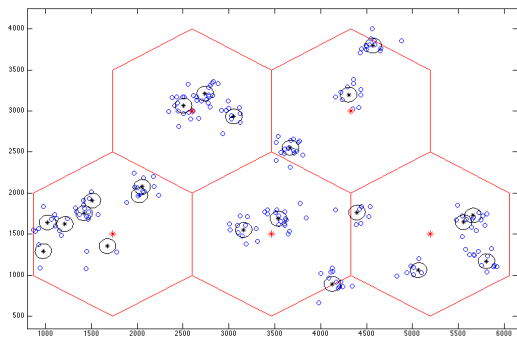


Fig. 15: Sample geographic distribution of users and WiFi APs. The black circles represent the range of a WiFi AP.

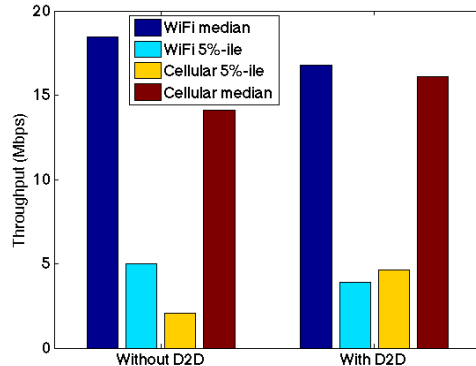


Fig. 16: Throughput changes in WiFi and cellular users when D2D cooperation is enabled.

the range of a given AP, then a user  $k$  at a distance  $d_k$  from the AP is offered a rate

$$R_k(t) = \kappa J_k(t) \min \left( R(d_k), \frac{R_{\max}}{N} \right),$$

where  $R(d)$  is a function that maps the user distance  $d$  from AP to the rate delivered to that user,  $R_{\max}$  is the maximum rate the AP can deliver,  $0 < \kappa \leq 1$  is a back-off factor capturing various non-idealities and overheads in the system, and  $J_k(t)$  is the binary variable that takes the value 0 if a neighbor of  $k$  in the connectivity graph is transmitting at time  $t$ , and 1 otherwise. We use the 802.11ac achievable rates reported in [31] (3 streams, 80MHz, with rates normalized to 40MHz) for the  $R(d_k)$  and  $R_{\max}$  values, with  $\kappa = 0.5$ . Since D2D transmissions can interfere with AP downlink, we reduce the device power to 17dBm for this setup. Our results under this setup are given in Figures 17 and 18. These plots provide throughput curves for the combined WiFi and cellular network, *i.e.*, if a user is served by WiFi, its throughput from WiFi is considered; otherwise, its throughput from the D2D-enhanced cellular network is considered.

The results suggest that when D2D cooperation and WiFi AP are simultaneously enabled, the performance is uniformly better than either of them individually enabled, despite the interference from D2D transmissions to AP users, and the relatively fewer D2D opportunities due to users being served by AP. We observe that the D2D gains concentrate more on the lower-end users compared to the gain due to WiFi and the reduced load at the base station. Note that this does not mean that the throughput of a given WiFi user is not reduced when D2D interference takes place; it means that, assuming the user falls within the bottom  $x$ -percentile of users after the



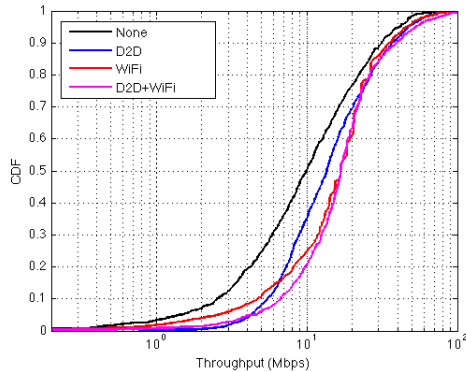


Fig. 17: Throughput CDF for large cells with APs, with  $\sigma = 100m$ .

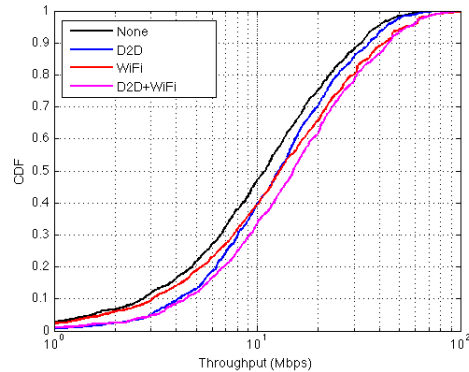


Fig. 18: Throughput CDF for large cells with APs, with  $\sigma = 200m$ .

D2D interference, they are still better off than the bottom  $x$ -percentile of users when only WiFi is enabled. Therefore overall, the combined benefit of WiFi and D2D strictly dominates the loss due to these transmissions interfering with each other. The fifth-percentile gain of the AP+D2D scenario versus the pure AP case is approximately  $1.8\times$ .

We also consider the individual throughput gains and losses of the median and bottom fifth-percentile WiFi and cellular users in Figure 16. We observe that the throughput loss of the WiFi users due to D2D interference is less than 10% and 20% respectively, for median and bottom fifth-percentile users, even though the throughput of the fifth-percentile cellular user has grown by 130% (note that the cell-edge gains are reduced because of more limited cooperation opportunities due to WiFi avoidance, but they are still significant). This is because D2D cooperation is used for a relatively small fraction of time compared to WiFi for a given user (see Figure 7), which limits the amount of interference caused to WiFi users.

We also observe that as the cluster radius standard deviation is increased so that the users become more dispersed, both gains reduce, since there are fewer users that are in AP range, and the average distance between users is larger and thus the D2D links are weaker.

### I. Co-existence with LTE-U

Note that the setup of the previous section can also be used to model the scenario with LTE-Unlicensed (LTE-U), where the APs are replaced with LTE-U-enabled small cells, and the delivered rates are adjusted accordingly. The slightly different interference avoidance mechanism of LTE-U [20] (compared to WiFi) is irrelevant here, since the D2D transmissions do not occur

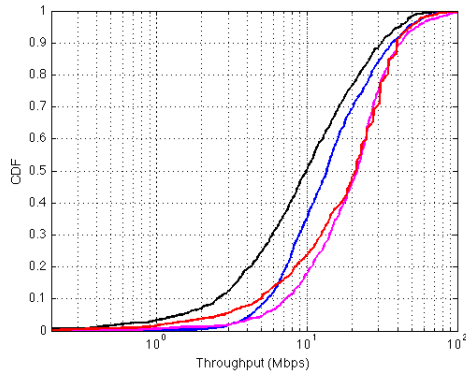


Fig. 19: Throughput CDF for D2D - LTE-U co-existence, with  $\sigma = 100m$ .

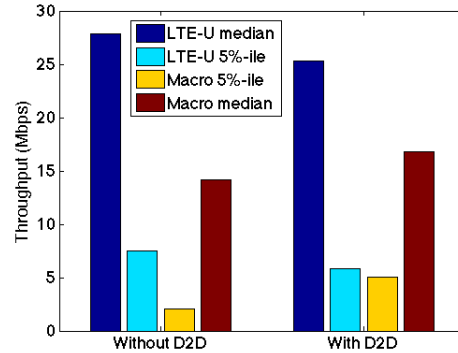


Fig. 20: Throughputs of LTE-U and macro base station users with and without D2D

within the range of the small cell and the LTE-U base station does not hear such transmissions (although an LTE-U user might overhear them, which is taken into account by assuming the LTE-U user loses any data sent in that time slot). Since LTE-U spectral efficiency is about  $1.6\times$  higher for medium traffic load compared to WiFi [32], we scale the variables  $R(d_k)$  and  $R_{\max}$  by this factor to model LTE-U rates.

The results under this setup are given in Figures 19, 20. We observe that the performance of the system where D2D and LTE-U are both enabled still mostly dominates the cases where each are individually enabled. The throughput losses in the median and bottom fifth-percentile LTE-U users are 9%, and 23%, respectively, while the gain of the bottom fifth-percentile macro base station user due to D2D cooperation is 150%.

### J. Co-existence with WiFi Off-loading

One can also consider an off-loading scenario where the base station continues serving the WiFi users. In this case, the WiFi users are still not available for D2D cooperation, but they can receive from both the AP and directly from the base station whenever they are scheduled based on their past throughputs. We compute the rate delivered to a WiFi user as the sum of the rate that is delivered from the base station (whenever scheduled) and the rate that is delivered from the AP. Figures 21 and 22 plot the throughput CDFs under this scenario. The results follow a similar pattern to the case where WiFi users are served only by the AP, with a small additional gain in the curves with AP off-loading.

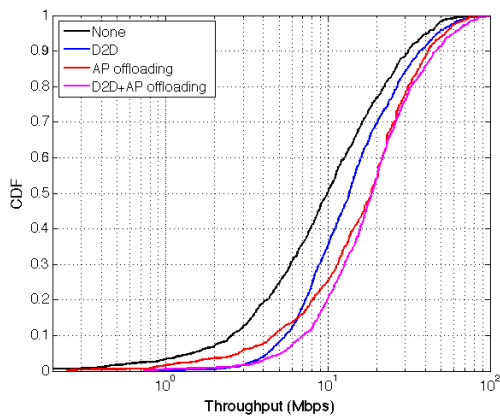


Fig. 21: Throughput CDF for large cells with APs, with  $\sigma = 100m$  (AP users served by AP and base station).

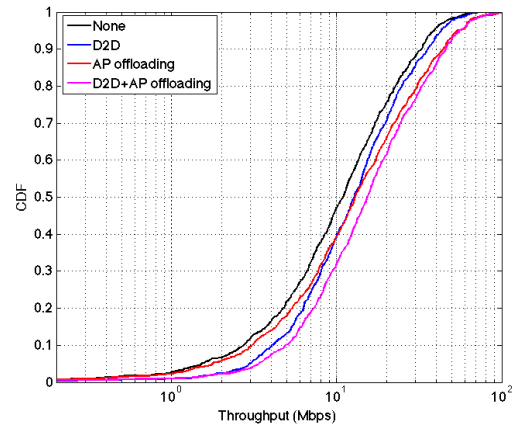


Fig. 22: Throughput CDF for large cells with APs, with  $\sigma = 200m$  (AP users served by AP and base station).

## VI. CONCLUSION

We proposed a cellular architecture that combines MU-MIMO downlink with opportunistic use of unlicensed ISM bands to establish device-to-device cooperation, which results in up to approximately  $6\times$  throughput gain in cell-edge users, while improving the overall throughput. In the physical layer, the architecture is based on using D2D relaying to form virtual MIMO channels. We proposed a scheduling algorithm for this architecture that activates such D2D links to extract opportunistic gains, while maintaining fairness in terms of both throughput and the amount of relaying. To this end, we introduced a novel utility function that incorporates the cost of relaying into scheduling. We studied the gains of the architecture through extensive simulations, which suggest significant throughput gains for both cell-edge and median users under various scenarios.

## REFERENCES

- [1] V. Tsibonis and L. Georgiadis, "Optimal downlink scheduling policies for slotted wireless time-varying channels," *IEEE Transactions on Wireless Communications*, vol. 4, no. 4, pp. 1808–1817, 2005.
- [2] P. P. Bhattacharya, L. Georgiadis, and P. Tsoucas, "Problems of adaptive optimization in multiclass M/GI/1 queues with Bernoulli feedback," *Mathematics of Operations Research*, vol. 20, no. 2, pp. 355–380, 1995.
- [3] G. Dimić and N. D. Sidiropoulos, "On downlink beamforming with greedy user selection: performance analysis and a simple new algorithm," *IEEE Transactions on Signal Processing*, vol. 53, no. 10, pp. 3857–3868, 2005.
- [4] A. Asadi, Q. Wang, and V. Mancuso, "A survey on device-to-device communication in cellular networks," *IEEE Communications Surveys & Tutorials*, vol. 16, no. 4, pp. 1801–1819, 2014.

- [5] A. Asadi and V. Mancuso, "On the compound impact of opportunistic scheduling and D2D communications in cellular networks," in *Proceedings of the 16th ACM International Conference on Modeling, Analysis & simulation of Wireless and Mobile Systems*, pp. 279–288, 2013.
- [6] T. Yoo and A. Goldsmith, "On the optimality of multiantenna broadcast scheduling using zero-forcing beamforming," *IEEE Journal on Selected Areas in Communications*, vol. 24, no. 3, pp. 528–541, 2006.
- [7] M. Sharif and B. Hassibi, "On the capacity of MIMO broadcast channels with partial side information," *IEEE Transactions on Information Theory*, vol. 51, no. 2, pp. 506–522, 2005.
- [8] H. Shirani-Mehr, G. Caire, and M. J. Neely, "MIMO downlink scheduling with non-perfect channel state knowledge," *IEEE Transactions on Communications*, vol. 58, no. 7, pp. 2055–2066, 2010.
- [9] L. Georgiadis, M. J. Neely, and L. Tassiulas, *Resource allocation and cross-layer control in wireless networks*. Now Publishers Inc., 2006.
- [10] A. Eryilmaz, A. Ozdaglar, and E. Modiano, "Polynomial complexity algorithms for full utilization of multi-hop wireless networks," in *26th IEEE International Conference on Computer Communications (INFOCOM)*, pp. 499–507, 2007.
- [11] E. Arikian, "Some complexity results about packet radio networks (corresp.)," *IEEE Transactions on Information Theory*, vol. 30, no. 4, pp. 681–685, 1984.
- [12] L. Tassiulas and A. Ephremides, "Stability properties of constrained queueing systems and scheduling policies for maximum throughput in multihop radio networks," *IEEE Transactions on Automatic Control*, vol. 37, no. 12, pp. 1936–1948, 1992.
- [13] L. Jiang and J. Walrand, "A distributed CSMA algorithm for throughput and utility maximization in wireless networks," *IEEE/ACM Transactions on Networking (ToN)*, vol. 18, no. 3, pp. 960–972, 2010.
- [14] E. Modiano, D. Shah, and G. Zussman, "Maximizing throughput in wireless networks via gossiping," in *ACM SIGMETRICS Performance Evaluation Review*, vol. 34, pp. 27–38, 2006.
- [15] H. Holm, G. E. Oien, M.-S. Alouini, D. Gesbert, and K. J. Hole, "Optimal design of adaptive coded modulation schemes for maximum average spectral efficiency," in *4th IEEE Workshop on Signal Processing Advances in Wireless Communications (SPAWC), 2003*, pp. 403–407, 2003.
- [16] A. D. Wyner and J. Ziv, "The rate-distortion function for source coding with side information at the decoder," *IEEE Transactions on Information Theory*, vol. 22, no. 1, pp. 1–10, 1976.
- [17] Y. Liang and V. V. Veeravalli, "Gaussian orthogonal relay channels: Optimal resource allocation and capacity," *IEEE Transactions on Information Theory*, vol. 51, no. 9, pp. 3284–3289, 2005.
- [18] S. Zahedi, M. Mohseni, and A. El Gamal, "On the capacity of AWGN relay channels with linear relaying functions," in *IEEE International Symposium on Information Theory (ISIT)*, pp. 399–399, 2004.
- [19] T. M. Cover and A. E. Gamal, "Capacity theorems for the relay channel," *IEEE Transactions on Information Theory*, vol. 25, no. 5, pp. 572–584, 1979.
- [20] R. Zhang, M. Wang, L. X. Cai, Z. Zheng, X. Shen, and L.-L. Xie, "LTE-unlicensed: the future of spectrum aggregation for cellular networks," *IEEE Wireless Communications*, vol. 22, no. 3, pp. 150–159, 2015.
- [21] A. S. Avestimehr, S. N. Diggavi, and D. N. Tse, "Wireless network information flow: A deterministic approach," *IEEE Transactions on Information Theory*, vol. 57, no. 4, pp. 1872–1905, 2011.
- [22] M. Duarte, A. Sengupta, S. Brahma, C. Fragouli, and S. Diggavi, "Quantize-map-forward (QMF) relaying: an experimental study," in *14th ACM International Symposium on Mobile Ad Hoc Networking and Computing*, pp. 227–236, 2013.
- [23] X. Lin, N. B. Shroff, and R. Srikant, "A tutorial on cross-layer optimization in wireless networks," *IEEE Journal on Selected Areas in Communications*, vol. 24, no. 8, pp. 1452–1463, 2006.
- [24] F. Kelly, "Charging and rate control for elastic traffic," *European Transactions on Telecommunications*, vol. 8, no. 1, pp. 33–37, 1997.

- [25] S. Rebennack, “Stable set problem: Branch & cut algorithms,” in *Encyclopedia of Optimization*, pp. 3676–3688, Springer, 2008.
- [26] V. Chvátal, “On certain polytopes associated with graphs,” *Journal of Combinatorial Theory, Series B*, vol. 18, no. 2, pp. 138–154, 1975.
- [27] B. Rosgen and L. Stewart, “Complexity results on graphs with few cliques,” *Discrete Mathematics and Theoretical Computer Science*, vol. 9, no. 1, 2007.
- [28] F. Gavril, “The intersection graphs of subtrees in trees are exactly the chordal graphs,” *Journal of Combinatorial Theory, Series B*, vol. 16, no. 1, pp. 47–56, 1974.
- [29] J. Salo, G. Del Galdo, J. Salmi, P. Kysti, M. Milojevic, D. Laselva, and C. Schneider, “MATLAB implementation of the 3GPP spatial channel model (3GPP TR 25.996), Jan. 2005. Available: [http://radio.aalto.fi/en/research/rf\\_applications\\_in\\_mobile\\_communications/propagation\\_research/matlab\\_scm\\_implementation/](http://radio.aalto.fi/en/research/rf_applications_in_mobile_communications/propagation_research/matlab_scm_implementation/)
- [30] “Study on LTE device to device proximity services; radio aspects”, 3GPP TR 36.843 V12.0.1, Mar 2014. Available: <http://www.3gpp.org/dynareport/36843.htm>
- [31] “Worlds first 5G WiFi 802.11ac SoC, Broadcom Corporation, 2012. Available: [https://www.broadcom.com/docs/press/80211ac\\_for\\_Enterprise.pdf](https://www.broadcom.com/docs/press/80211ac_for_Enterprise.pdf)
- [32] “U-LTE: Unlicensed spectrum utilization of LTE,” tech. rep., Huawei whitepaper.

## APPENDIX A

### PROOF OF THEOREM 4

**Proposition 1.** *Let  $X_i, i = 1, \dots, n$ , be i.i.d.  $\chi^2(2P)$  random variables. Then*

$$\mathbb{P} \left( \min_{1 \leq i \leq n} X_i > n^{-\frac{\gamma}{2P}} g(2P) \right) = O \left( e^{-n^{1-\gamma}} \right), \text{ for } 0 < \gamma < 1.$$

*Proof:* Using the Taylor series for the upper incomplete Gamma function, as  $x \rightarrow 0$ ,

$$\mathbb{P}(X_i > x) = 1 - \frac{x^{2P}}{(2P)!} + O(x^{2P+1}).$$

Therefore,

$$\mathbb{P} \left( \min_{1 \leq i \leq n} X_i > n^{-\frac{\gamma}{2P}} g(2P) \right) = \left( \mathbb{P} \left( X_i > n^{-\frac{\gamma}{2P}} g(2P) \right) \right)^n = (1 - n^{-\gamma})^n = O \left( e^{-n^{1-\gamma}} \right). \quad \blacksquare$$

We will first derive a lower bound on  $\text{SNR}_{ij}^{\text{coop}}$ , defined by  $\text{SNR}_{ij}^{\text{coop}} = \frac{s_{ij1}^2}{1 + |u_{ijk}(2)|^2 \frac{\sigma_j^2}{\|\tilde{g}_{ij}\|^2}}$ . Using the fact that  $|u_{ijk}(2)|^2 \leq 1$  and  $\sigma_{j|i}^2 \leq \sigma_j^2$ , where  $\sigma_j^2$  is the variance of  $y_2$ ,

$$\text{SNR}_{ij}^{\text{coop}} \geq \frac{s_{ij1}^2}{1 + \frac{\sigma_j^2}{\|\tilde{g}_{ij}\|^2}} = \frac{s_{ij1}^2}{1 + \frac{1 + \|\mathbf{h}_j\|^2}{\|\tilde{g}_{ij}\|^2}}. \quad (17)$$

Next, since  $s_{ij1}^2$  is the larger eigenvalue of the matrix  $\mathbf{H}_{ij} \mathbf{H}_{ij}^*$ , using the closed form expressions for the eigenvalues of  $2 \times 2$  matrices,

$$s_{ij1}^2 = \frac{1}{2} \left( \|\mathbf{h}_i\|^2 + \|\mathbf{h}_j\|^2 + \sqrt{\|\mathbf{h}_i\|^4 + \|\mathbf{h}_j\|^4 + 2\|\mathbf{h}_i\|^2\|\mathbf{h}_j\|^2 \cos(2\Theta)} \right)$$

$$\geq \frac{1}{2} (\|\mathbf{h}_i\|^2 + \|\mathbf{h}_j\|^2 + |\|\mathbf{h}_i\|^2 - \|\mathbf{h}_j\|^2|) = \max(\|\mathbf{h}_i\|^2, \|\mathbf{h}_j\|^2),$$

where  $\Theta = \cos^{-1} \frac{\mathbf{h}_i^* \mathbf{h}_j}{\|\mathbf{h}_i\| \|\mathbf{h}_j\|}$  is the angle between  $\mathbf{h}_i$  and  $\mathbf{h}_j$ , and the lower bound is obtained by setting  $\cos(2\Theta) = -1$ . Using this lower bound in (17), we get

$$\begin{aligned} \text{SNR}_{ij}^{\text{coop}} &\geq \frac{\max(\|\mathbf{h}_i\|^2, \|\mathbf{h}_j\|^2)}{1 + \frac{1 + \|\mathbf{h}_j\|^2}{\|\check{g}_{ij}\|^2}} \geq \frac{\|\mathbf{h}_j\|^2}{1 + \frac{1 + \|\mathbf{h}_j\|^2}{\|\check{g}_{ij}\|^2}} \geq \frac{(\|\mathbf{h}_j\|^2 + 1) \|\check{g}_{ij}\|^2}{1 + \|\mathbf{h}_j\|^2 + \|\check{g}_{ij}\|^2} - 1 \\ &\geq \frac{1}{2} \min(\|\mathbf{h}_j\|^2, \|\check{g}_{ij}\|^2) - 1. \end{aligned}$$

Therefore, to prove the first claim in Theorem 4, it is sufficient to prove that

$$\mathbb{P} \left( \min_{i \in \mathcal{N}} \min(\|\mathbf{h}_{j^*(i)}\|^2, \|\check{g}_{ij^*(i)}\|^2) > M\rho \left( \frac{1}{2} \log n - 2 \log \log n \right) \right) = O \left( e^{-\log^2 n + 2 \log n} \right).$$

Define  $\mathcal{P}_n = \{j : \|\mathbf{h}_j\|^2 \geq M\rho \left( \frac{1}{2} \log n - 2 \log \log n \right)\}$ , and  $\mathcal{R}_n(i) = \{j \in \mathcal{P}_n : \phi_{ij} \geq n^{\frac{\alpha}{4}}\}$ .

**Proposition 2.**  $\mathbb{P}(\mathcal{R}_n(i) = \emptyset \text{ for some } i) = O \left( e^{-\log^2 n + 2 \log n} \right)$ .

Therefore, if  $\mathcal{R}_n(i) \neq \emptyset$  for all  $i$ ,

$$\begin{aligned} 1 + \text{SNR}_{\min}^{\text{coop}} &\geq \frac{1}{2} \min_{i \in \mathcal{N}} \min(\|\mathbf{h}_{j^*(i)}\|^2, \|\check{g}_{ij^*(i)}\|^2) \\ &\geq \frac{1}{2} \min_{i \in \mathcal{N}} \min \left( M\rho \left( \frac{1}{2} \log n - 2 \log \log n \right), n^{\frac{\alpha}{4}} \|\nu_{ij^\dagger(i)}\|^2 \right) \\ &= \frac{1}{2} \min \left( M\rho \left( \frac{1}{2} \log n - 2 \log \log n \right), n^{\frac{\alpha}{4}} \min_{i \in \mathcal{N}} \|\nu_{ij^\dagger(i)}\|^2 \right), \end{aligned}$$

where  $j^\dagger(i) = \arg \max_{j \in \mathcal{R}_n(i)} \mathbb{E} [\text{SNR}_{ij}^{\text{coop}} | \phi_{ij}, \mathbf{h}_j]$ , and thus

$$\mathbb{P} \left( \text{SNR}_{\min}^{\text{coop}} < \frac{1}{2} M\rho \left( \frac{1}{2} \log n - 2 \log \log n \right) - 1 \mid \mathcal{R}_n(i) \neq \emptyset \forall i \right) = O \left( e^{-n^{1-\gamma}} \right), \quad (18)$$

for all  $0 < \gamma < 1$ , by Proposition 1, by the fact that  $\|\nu_{ij}\|^2$  is a  $\chi^2(2)$  random variable, and that  $j^\dagger(i)$  is independent of  $\|\nu_{ij}\|^2$ . Then (18), together with Proposition 2 implies the first claim of the theorem.

It remains to prove Proposition 2. To achieve this, we will first lower bound the tail probability  $\mathbb{P}(\|\mathbf{h}_j\|^2 > a)$ . Define  $\hat{\mathbf{e}}_{j,k} := \frac{\mathbf{e}_{j,k}}{\|\mathbf{e}_{j,k}\|} = \frac{\mathbf{e}_{j,k}}{\sqrt{M}}$ ,  $\mathbf{E}_j := [\hat{\mathbf{e}}_{j,1} \dots \hat{\mathbf{e}}_{j,P}]$ , and  $\alpha_j := [\alpha_{j,k}]_k$ . Letting  $\mathbf{E}_j = \mathbf{Q}_j \Lambda_j \mathbf{Q}_j^*$  be an eigendecomposition of  $\mathbf{E}_j$ ,

$$\begin{aligned} \|\mathbf{h}_j\|^2 &= \rho \left\| \sum_{k=1}^P \alpha_{j,k} \mathbf{e}(\theta_{j,k}) \right\|^2 = M\rho \left\| \sum_{k=1}^P \alpha_{j,k} \hat{\mathbf{e}}(\theta_{j,k}) \right\|^2 \\ &= M\rho (\mathbf{E}_j \alpha_j)^* (\mathbf{E}_j \alpha_j) = M\rho \alpha_j^* (\mathbf{E}_j^* \mathbf{E}_j) \alpha_j = M\rho \sum_{k=1}^P \lambda_k (\mathbf{E}_j^* \mathbf{E}_j) |(\mathbf{Q}_j \alpha_j)_k|^2, \end{aligned}$$

where  $\lambda_k(\mathbf{E}_j^* \mathbf{E}_j)$  is the  $k$ th eigenvalue of  $\mathbf{E}_j^* \mathbf{E}_j$ , and  $(\mathbf{Q}_j \alpha_j)_k$  is the  $k$ th element of  $\mathbf{Q}_j \alpha_j$ . Since  $\sum_{k=1}^P \lambda_k(\mathbf{E}_j^* \mathbf{E}_j) = \text{tr}(\mathbf{E}_j^* \mathbf{E}_j) = P$ , there must exist a  $k$ , say  $k^*$ , such that  $\lambda_{k^*}(\mathbf{E}_j^* \mathbf{E}_j) \geq 1$ . Hence,

$$\|\mathbf{h}_j\|^2 = M\rho \sum_{k=1}^P \lambda_k(\mathbf{E}_j^* \mathbf{E}_j) |(\mathbf{Q}_j \alpha_j)_k|^2 \geq M\rho |(\mathbf{Q}_j \alpha_j)_{k^*}|^2.$$

Since  $\mathbf{E}_j$  is independent from  $\alpha_j$ , and since the distributions of i.i.d. Gaussian vectors are invariant under orthogonal transformations,  $|(\mathbf{Q}_j \alpha_j)_{k^*}|^2$  has the same distribution as  $\|\alpha_{j,k}\|^2$  for an arbitrary  $k$ , i.e.,  $\chi^2(2)$  distribution, or equivalently, exponential distribution with mean 1. Therefore, the tail probability of  $\|\mathbf{h}_j\|^2$  can be lower bounded by  $\mathbb{P}(\|\mathbf{h}_j\|^2 > M\rho a) \geq e^{-a}$ . Hence,

$$\mathbb{P}(|\mathcal{P}_n| \leq (1-\delta)\sqrt{n}) = \mathbb{P}\left(\sum_{j=1}^n \mathbb{I}\left(\|\mathbf{h}_j\|^2 \geq M\rho \left(\frac{1}{2} \log n - 2 \log \log n\right)\right)\right) \leq (1-\delta)\sqrt{n}$$

Using the tail lower bound on  $\|\mathbf{h}_j\|^2$ , we see that each indicator variable is i.i.d. with mean at least  $\frac{\log^2 n}{\sqrt{n}}$ . Therefore, using Chernoff bound,

$$\mathbb{P}(|\mathcal{P}_n| \leq (1-\delta)\sqrt{n} \log^2 n) \leq O\left(e^{-\delta^2 \sqrt{n} \log^2 n}\right)$$

Next, we consider the probability  $\mathbb{P}(\mathcal{R}_n(1) = \emptyset \mid |\mathcal{P}_n| \geq (1-\delta)\sqrt{n} \log^2 n)$ . Since the users are uniformly distributed in a circle of radius  $R$ ,  $\mathbb{P}(r_{ij} \leq r) = \frac{r^2}{R^2}$  for sufficiently small  $r > 0$ , and consequently  $\mathbb{P}(\phi_{ij} \geq x) = \frac{1}{R^2} x^{-\frac{2}{\alpha}}$ . Since  $h_j$  is independent from  $\phi_{1j}$ ,

$$\begin{aligned} \mathbb{P}(\mathcal{R}_n(1) = \emptyset \mid |\mathcal{P}_n| \geq (1-\delta)\sqrt{n} \log^2 n) &= \left(1 - \mathbb{P}(\phi_{1j} \geq n^{\frac{\alpha}{4}})\right)^{(1-\delta)\sqrt{n} \log^2 n} \\ &= \left(1 - n^{-\frac{1}{2}}\right)^{(1-\delta)\sqrt{n} \log^2 n} = O\left(e^{-(1-\delta) \log^2 n}\right). \end{aligned}$$

Then, choosing  $\delta = \frac{1}{\log n}$ , and by using independence of channels across  $i$ 's,

$$\mathbb{P}(\mathcal{R}_n(1) \neq \emptyset \ \forall i) = \left(1 - O\left(e^{-(1-\delta) \log^2 n}\right) - O\left(e^{-\delta^2 \sqrt{n} \log^2 n}\right)\right)^n = 1 - O\left(e^{-\log^2 n + 2 \log n}\right)$$

which concludes our proof of the first claim.

To prove the second claim, we note that

$$\|h_i\|^2 = \rho \left\| \sum_{k=1}^P \alpha_{i,k} \mathbf{e}(\theta_{i,k}) \right\|^2 \leq \rho \sum_{k=1}^P |\alpha_{i,k}|^2 \|\mathbf{e}(\theta_{i,k})\|^2 = M\rho X_i,$$

where  $X_i \sim \chi^2(2P)$ . The second claim then follows by Proposition 1.

## APPENDIX B

## PROOF OF LEMMA 2

Define  $y^Q = \sum_{(i,j) \in Q} \sum_{s: \substack{i \in s_1 \\ j \in s_2}} \sum_{k \in K} \sum_{\ell \in L} y_{sk\ell}$ , and consider the following sequence of optimization problems, indexed by  $n$  (with a slight abuse of notation):

$$\text{maximize } U_n(\mathbf{y}) := \sum_{i \in \mathcal{N}} U_i(\mathbf{y}) - \sum_{Q \in \mathcal{Q}} \exp\{n(y^Q - 1)\} \quad (19)$$

$$\text{s.t. } y_{sk\ell} \geq 0, \quad \sum_s y_{sk\ell} \leq p_k q_\ell, \quad y_{sk\ell} = q_\ell \sum_{\ell'} y_{sk\ell'}, \quad \forall s, k, \ell. \quad (20)$$

We will denote the optimal value of the optimization (19) with  $\text{OPT}_n$ . Further consider the corresponding sequence of scheduling policies  $\pi_n$ , that choose  $s^* = \arg \max_{s \subseteq \mathcal{N}^2 \times \{1,2\}} \tilde{f}_n(s)$ , where

$$\tilde{f}_n(s) = \sum_{(i,j,m) \in s} \mathbb{E} \left[ R_{sK(t)L(t)}^{(i)} \right] \frac{\partial U_i}{\partial r_i} \Big|_{r_i=r_i(t-1)} + \frac{\partial U_j}{\partial \beta_j} \Big|_{r_j=r_j(t-1)} - n \sum_{Q: s_{12} \cap Q \neq \emptyset} e^{n(y^Q(t)-1)}, \quad (21)$$

The empirical utility of the policy  $\pi_n$  up to time  $t$  is denoted by  $U_n(t)$ .

**Proposition 3.**  $\lim_{n \rightarrow \infty} \text{OPT}_n = \text{OPT}'$ .

*Proof:* We first show that for any  $\epsilon > 0$ ,  $\text{OPT}_n \geq \text{OPT}' - \epsilon$  for large enough  $n$ . Consider the optimization (14), with the condition (16) replaced by

$$y^Q \leq 1 + \Delta, \quad \forall Q \in \mathcal{Q}, \quad (22)$$

and denote the optimal value of the resulting maximization as  $\text{OPT}^\Delta$ . By continuity of the objective function, for any  $\epsilon > 0$ , there exists  $\delta > 0$  such that  $|\text{OPT}^{-\delta} - \text{OPT}'| < \frac{\epsilon}{2}$ . For such  $\delta$ , choose  $n$  large enough so that  $e^{-n\delta} < \frac{\epsilon}{2|\mathcal{Q}|}$ . Similarly, denote the maximal value of (19) subject to (22) as  $\text{OPT}_n^\Delta$ . Then

$$\text{OPT}_n \geq \text{OPT}_n^{-\delta} \geq \text{OPT}^{-\delta} - \frac{\epsilon}{2} \geq \text{OPT}' - \epsilon.$$

Next, we show that for large enough  $n$ ,  $\text{OPT}_n \leq \text{OPT}' + \epsilon$ . Choose  $\delta > 0$  small enough so that  $|\text{OPT}^\delta - \text{OPT}'| < \epsilon$ . Hence

$$\text{OPT}' + \epsilon \geq \text{OPT}^\delta \geq \text{OPT}_n^\delta.$$

Therefore it is sufficient to show that  $\text{OPT}_n^\delta = \text{OPT}_n$  for large enough  $n$ . If we choose  $n$  large enough so that

$$\frac{\partial U_n(\mathbf{y})}{\partial y^Q} \Big|_{y^Q > 1+\delta} = \sum_{i \in \mathcal{N}} \frac{\partial U_i(\mathbf{y})}{\partial y^Q} - n e^{n(y^Q-1)} \Big|_{y^Q > 1+\delta} < 0,$$



then concavity implies  $\text{OPT}_n^\delta = \text{OPT}_n$ , since the derivative would have to be monotonically decreasing with increasing  $y^Q$ . Such a choice of  $n$  is possible since  $\left. \frac{\partial U_i(\mathbf{y})}{\partial y^Q} \right|_{y^Q=1+\delta} < \infty$ , similarly by concavity and twice continuous differentiability, which concludes the proof. ■

**Proposition 4.**  $\lim_{n \rightarrow \infty} U_n(t) = U(t)$ .

*Proof:* It is sufficient to show that for a given  $t$ , for a sufficiently large  $n$ , all the control actions taken by policies  $\pi_n$  and  $\pi^*$  up to time  $t$  are identical. Note that since the sets  $\mathcal{K}$ ,  $\mathcal{L}$  and  $\mathcal{N}$  are finite, for a finite  $t$ , there are finitely many values  $y_{sk\ell}(t)$ , and therefore  $f_s(t)$  can take. Therefore we can choose  $n$  large enough so that

- 1) For any  $\tau \leq t$ , if  $y^Q(\tau) > 1$  for some  $Q$ , then

$$f_s(\tau) - n \exp\{n(y^Q - 1)\} < f_{s^*}(\tau)$$

for all subsets  $s$  such that  $s_{12} \cap Q \neq \emptyset$ ,

- 2) For each pair of subsets  $s, t \subseteq \bar{\mathcal{N}}(t) \times \{1, 2\}$  such that  $f_s(\tau) > f_t(\tau)$  and  $y^Q(\tau) < 1$  for all  $Q$  s.t.  $s_{12} \cap Q \neq \emptyset$  and  $t_{12} \cap Q \neq \emptyset$ ,

$$f_s(\tau) - n \sum_{Q: s_{12} \cap Q \neq \emptyset} \exp\{n(y^Q(\tau) - 1)\} > f_t(\tau) - n \sum_{Q: t_{12} \cap Q \neq \emptyset} \exp\{n(y^Q(\tau) - 1)\}.$$

Here, the first condition ensures that a subset that violates any of the clique constraints is never scheduled, and the second condition ensures that for the subsets whose scheduling does not violate any of the clique constraints, the order with respect to  $f$  is preserved, and hence the subset that maximizes  $f$  remains the same. This is possible since for  $x > 0$ ,  $e^{nx}$  can be made arbitrarily large, whereas for  $x < 0$ , it can be made arbitrarily small by scaling  $n$ . For such  $n$ , all scheduling decisions of  $\pi^*$  and  $\pi_n$  up to time  $t$  are identical, and thus  $U_n(t) = U(t)$  for  $n$  sufficiently large. ■

**Proposition 5.**  $\lim_{t \rightarrow \infty} U_n(t) = \text{OPT}_n$ .

*Proof:* The proof uses Lyapunov optimization techniques from [2], [1]. We will make use of the following theorem from [2] to show the result.

**Theorem 7.** Consider a stochastic sequence in  $\mathbb{R}^p$  satisfying the recursion

$$\mathbf{y}(t) = \mathbf{y}(t-1) + \frac{1}{t} \mathbf{g}(t),$$

and let  $\{\mathcal{F}_t\}_{t \geq 0}$  be a non-decreasing family of filtrations of the underlying  $\sigma$ -algebra, such that  $\mathbf{g}(t)$  is  $\mathcal{F}_t$ -measurable.

Assume the following are satisfied.

1) There exists a compact set  $\mathcal{A} \subseteq \mathbb{R}^p$  such that

$$\liminf_{t \rightarrow \infty} \{\|\mathbf{y}(t) - \mathbf{y}\|_1 : \mathbf{y} \in \mathcal{A}\} = 0,$$

2) There exists  $K > 0$  such that for all  $t$ ,  $\|\mathbf{g}(t)\|_1 \leq K$ ,

3) There exists a twice continuously differentiable function  $V : \mathbb{R}^p \rightarrow \mathbb{R}$  such that

$$\mathbb{E} [\mathbf{g}^\top(t+1) | \mathcal{F}_t] \nabla V(\mathbf{y}(t)) < -V(\mathbf{y}(t)),$$

where  $^\top$  represents vector transpose.

Then the function  $V$  in condition 3 satisfies  $\lim_{t \rightarrow \infty} V(\mathbf{y}(t))^+ = 0$ .

Consider the sequence of vectors  $\mathbf{y}(t) = \{y_{sk\ell}(t)\}_{s,k,\ell}$ , whose entries satisfy the recursion

$$y_{sk\ell}(t) = y_{sk\ell}(t-1) + \frac{1}{t} (\mathbb{I}_{S(t)=s} \mathbb{I}_{K(t)=k} \mathbb{I}_{L(t)=\ell} - y_{sk\ell}(t-1)).$$

Note that the vector  $\mathbf{y}(t)$  converges to the compact set defined by (15)–(16), by the first claim of Theorem 6, and the entries of the corresponding update sequence  $\mathbf{g}(t)$  in this case is bounded by 1. Following the strategy of [1], we choose

$$\begin{aligned} V(\mathbf{y}(t)) &= \sum_{i \in \mathcal{N}} U_i \left( \sum_{s:i \in s_1} \sum_{k \in \mathcal{K}} \sum_{\ell \in \mathcal{L}} R_{sk\ell}^{(i)} y_{sk\ell}^*, \sum_{s:i \in s_2} \sum_{k \in \mathcal{K}} \sum_{\ell \in \mathcal{L}} y_{sk\ell}^* \right) - \sum_{Q \in \mathcal{Q}} \exp \{n(y^{*Q} - 1)\} \\ &\quad - \sum_{i \in \mathcal{N}} U_i \left( \sum_{s:i \in s_1} \sum_{k \in \mathcal{K}} \sum_{\ell \in \mathcal{L}} R_{sk\ell}^{(i)} y_{sk\ell}(t), \sum_{s:i \in s_2} \sum_{k \in \mathcal{K}} \sum_{\ell \in \mathcal{L}} y_{sk\ell}(t) \right) + \sum_{Q \in \mathcal{Q}} \exp \{n(y^Q(t) - 1)\}, \end{aligned}$$

where  $\mathbf{y}^*$  is the solution to (19)<sup>14</sup>. Then, if we verify the third condition for this choice of  $V$ , then the proof is concluded using Theorem 7.

We first evaluate the terms in the left-hand side of the third condition.

$$\begin{aligned} \mathbb{E} [g_{sk\ell}^\top(t+1) | \mathcal{F}_t] &= \mathbb{E} [\mathbb{I}_{S(t+1)=s} \mathbb{I}_{K(t+1)=k} \mathbb{I}_{L(t+1)=\ell} | \mathcal{F}_t] - y_{sk\ell}(t) \\ &= \sum_{b \in \mathcal{K}, c \in \mathcal{L}} \mathbb{E} [\mathbb{I}_{S(t+1)=s} \mathbb{I}_{K(t+1)=k} \mathbb{I}_{L(t+1)=\ell} | K(t+1) = b, L(t+1) = c, \mathcal{F}_t] p_b q_c - y_{sk\ell}(t) \\ &= \mathbb{E} [\mathbb{I}_{S(t+1)=s} | K(t+1) = k, L(t+1) = \ell, \mathcal{F}_t] p_k q_\ell - y_{sk\ell}(t) = \begin{cases} p_k q_\ell - y_{sk\ell}(t), & \text{if } s = s^*, \\ -y_{sk\ell}(t), & \text{otherwise} \end{cases} \end{aligned}$$

<sup>14</sup>Since (19) is the maximization of a continuous function over a compact set, the extreme values are attained within the feasible set.

where  $s^* = \arg \max_{\tilde{s} \in \bar{\mathcal{N}}(t+1) \times \{1,2\}} \tilde{f}_n(\tilde{s})$ . Since a single entry of  $\nabla V(\mathbf{y}(t))$  is given by

$$D_{skl} := \frac{\partial V(\mathbf{y}(t))}{\partial y_{skl}(t)} = - \sum_{i \in s_1} R_{skl}^{(i)} \frac{\partial U_i}{\partial r_i} \Big|_{r_i=r_i(t)} - \sum_{i \in s_2} \frac{\partial U_i}{\partial \beta_i} \Big|_{\beta_i=\beta_i(t)} + n \sum_{(i,j) \in s_{12}} \sum_{Q:(i,j) \in Q} e^{n(y^Q(t)-1)},$$

and the inner product on the left-hand side of the third condition can be expressed as

$$\begin{aligned} \mathbb{E} [g^\top(t+1) | \mathcal{F}_t] \nabla V(\mathbf{y}(t)) &= - \sum_{k \in \mathcal{K}} \sum_{\ell \in \mathcal{L}} D_{s^*k\ell} p_k q_\ell + \sum_{k \in \mathcal{K}} \sum_{\ell \in \mathcal{L}} \sum_s D_{skl} y_{skl}(t) \\ &= - \sum_{k \in \mathcal{K}} \mathbb{E}_L [D_{s^*kL}] p_k + \sum_{k \in \mathcal{K}} \sum_{\ell \in \mathcal{L}} \sum_s D_{skl} y_{skl}(t) \\ &\leq - \sum_{k \in \mathcal{K}} \sum_{\ell \in \mathcal{L}} \sum_s \mathbb{E}_L [D_{s^*kL}] y_{skl}^* + \sum_{k \in \mathcal{K}} \sum_{\ell \in \mathcal{L}} \sum_s D_{skl} y_{skl}(t) \\ &\leq - \sum_{k \in \mathcal{K}} \sum_{\ell \in \mathcal{L}} \sum_s \mathbb{E}_L [D_{skL}] y_{skl}^* + \sum_{k \in \mathcal{K}} \sum_{\ell \in \mathcal{L}} \sum_s D_{skl} y_{skl}(t) \\ &\leq - \sum_{k \in \mathcal{K}} \sum_{\ell \in \mathcal{L}} \sum_s \sum_{\ell' \in \mathcal{L}} q_{\ell'} D_{sk\ell'} y_{sk\ell'}^* + \sum_{k \in \mathcal{K}} \sum_{\ell \in \mathcal{L}} \sum_s D_{skl} y_{skl}(t) \\ &\stackrel{(a)}{=} - \sum_{k \in \mathcal{K}} \sum_s \sum_{\ell' \in \mathcal{L}} D_{sk\ell'} y_{sk\ell'}^* + \sum_{k \in \mathcal{K}} \sum_{\ell \in \mathcal{L}} \sum_s D_{skl} y_{skl}(t) \\ &= - \sum_{k \in \mathcal{K}} \sum_s \sum_{\ell \in \mathcal{L}} \frac{\partial V(\mathbf{y}(t))}{\partial y_{skl}(t)} (y_{skl}^* - y_{skl}(t)) \stackrel{(b)}{\leq} -V(\mathbf{y}(t)) \end{aligned}$$

where (a) follows by the second constraint in (20), and (b) follows by convexity.  $\blacksquare$

Finally, we can prove that  $U(t) \rightarrow \text{OPT}'$ . Note that this is equivalent to the statement

$$\lim_{n \rightarrow \infty} \lim_{t \rightarrow \infty} U_n(t) = \lim_{t \rightarrow \infty} \lim_{n \rightarrow \infty} U_n(t).$$

Given  $\epsilon > 0$ , using Propositions 3, 4 and 5, we can find sufficiently large  $n$  and  $t$  such that

$$|U(t) - \text{OPT}| \leq |U(t) - U_n(t)| + |U_n(t) - \text{OPT}_n| + |\text{OPT}_n - \text{OPT}| < \frac{\epsilon}{3} + \frac{\epsilon}{3} + \frac{\epsilon}{3} = \epsilon,$$

which concludes the proof.

## APPENDIX C

### PROOF OF THEOREM 2

*Proof:* The upper bound follows by the fact that  $\tilde{C}$  is an upper bound on the capacity. To prove the lower bound, we first note that for any input covariance matrix  $\mathbf{Q}$ ,

$$\sigma_{2|1}^2 = \frac{|\Sigma|}{\Sigma_{11}} = \frac{|\mathbf{I} + \mathbf{H}\mathbf{Q}\mathbf{H}^*|}{1 + \|\mathbf{h}_1\|^2}, \quad (23)$$

and that  $\mathbf{K}^{-1} = \text{diag}(1, \eta)$ , where  $\eta = \frac{1}{1 + \frac{\sigma_{2|1}^2}{2^{\bar{R}_{12}} - 1}}$ . Next, we lower bound  $R_{\text{MIMO}}$  as follows.

$$R_{\text{MIMO}} = \log |\mathbf{I}_2 + \mathbf{K}^{-1} \mathbf{H} \mathbf{Q} \mathbf{H}^*| \stackrel{\text{(a)}}{\geq} \log |\mathbf{K}^{-1} + \mathbf{K}^{-1} \mathbf{H} \mathbf{Q} \mathbf{H}^*| \geq \log |\mathbf{I}_2 + \mathbf{H} \mathbf{Q} \mathbf{H}^*| + \log \eta, \quad (24)$$

To see why (a) holds, define  $\mathbf{P} := \mathbf{K}^{-1} - \mathbf{I}_2$ , and denote by  $\lambda_k(\mathbf{A})$  the  $k$ 'th largest eigenvalue for a matrix  $\mathbf{A}$ . Then by Weyl's inequality, since  $\eta \leq 1$ ,

$$\lambda_k(\mathbf{P} + \mathbf{I}_2 + \mathbf{K}^{-1} \mathbf{H} \mathbf{Q} \mathbf{H}^*) \leq \lambda_k(\mathbf{I}_2 + \mathbf{K}^{-1} \mathbf{H} \mathbf{Q} \mathbf{H}^*) + \lambda_1(\mathbf{P}) = \lambda_k(\mathbf{I}_2 + \mathbf{K}^{-1} \mathbf{H} \mathbf{Q} \mathbf{H}^*),$$

which implies latter determinant in (24) is smaller. Next, note that  $\eta$  can be lower bounded by

$$\eta \leq \begin{cases} \frac{2^{\bar{R}_{12}} - 1}{2\sigma_{2|1}^2} & \text{if } \sigma_{2|1}^2 \geq 2^{\bar{R}_{12}} - 1 \\ \frac{1}{2} & \text{otherwise} \end{cases} \quad (25)$$

Then, combining (23), (24), and (25), we can show that  $R_{\text{MIMO}}$  is lower bounded by

$$R_{\text{MIMO}} \geq \min \left\{ \max_{\text{tr}(\mathbf{Q}) \leq 1} \log |\mathbf{I}_2 + \mathbf{H} \mathbf{Q} \mathbf{H}^*|, \log(1 + \|\mathbf{h}_1\|^2) + \log^+(2^{\bar{R}_{12}} - 1) \right\} - 1,$$

where  $\log^+(x) := \max(0, \log(x))$ . We conclude the proof by noting that for any  $x \geq 0$ ,  $\log^+(x) \geq \log(1 + x) - 1$ . ■